NASA TECHNICAL NOTE

NASA TN D-5859

NASA TN D-5859

GEOMETRIC PROPERTIES OF A MODIFIED WHIRLING-MEMBRANE SOLAR-ENERGY CONCENTRATOR

by John M. Jerke and Atwood R. Heath, Jr.

Langley Research Center
Hampton, Va. 23365

NATIONAL AERONAUTICS AND SPACE ADMINISTRATION • WASHINGTON, D. C. • JUNE 1970

1. Report No.	2. Government Accession No.	3. Recipient's Catalog No.
NASA TN D-5859		

4. Title and Subtitle	5. Report Date
GEOMETRIC PROPERTIES OF A MODIFIED WHIRLING-MEMBRANE SOLAR-ENERGY CONCENTRATOR	June 1970
	6. Performing Organization Code
7. Author(s)	8. Performing Organization Report No.
John M. Jerke and Atwood R. Heath, Jr.	L-6837
	10. Work Unit No.
9. Performing Organization Name and Address	120-33-17-08
NASA Langley Research Center Hampton, Va. 23365	11. Contract or Grant No.
	13. Type of Report and Period Covered
12. Sponsoring Agency Name and Address	Technical Note
National Aeronautics and Space Administration Washington, D.C. 20546	14. Sponsoring Agency Code

15. Supplementary Notes

16. Abstract

The geometry of three modified paraboloidal whirling-membrane solar-concentrator models of 3.05-m diameter was measured by using an optical-ray-trace technique. The membranes were fabricated of 0.01-mm-thick aluminized plastic, attached to metal hubs, and rotated at 71 rad/s in a vacuum chamber. Geometric properties such as focal length, mean and standard-deviation errors, and geometric efficiency for three models with different metal-hub diameters are discussed and compared with results for a similar whirling-membrane model of an earlier investigation.

17. Key Words (Suggested by Author(s))	18. Distribution Statement
Solar-energy concentrator Whirling membrane Expandable solar concentrator	Unclassified – Unlimited

19. Security Classif. (of this report)	20. Security Classif. (of this page)	21. No. of Pages	22. Price*
Unclassified	Unclassified	42	$3.00

*For sale by the Clearinghouse for Federal Scientific and Technical Information
Springfield, Virginia 22151

GEOMETRIC PROPERTIES OF A MODIFIED WHIRLING-MEMBRANE SOLAR-ENERGY CONCENTRATOR

By John M. Jerke and Atwood R. Heath, Jr.
Langley Research Center

SUMMARY

The whirling-membrane solar concentrator has been proposed for use with spacecraft-power-conversion devices because of its compact-packaging potential. Three membranes of 0.01-mm-thick aluminized plastic were constructed and attached to metal hubs for which the ratios of hub radius to membrane radius were 0.20, 0.35, and 0.50. The resulting models with design focal lengths of 132.1 cm and design diameters of 3.05 m were rotated at 71 rad/s in a vacuum chamber at pressures below 133 N/m^2. The present models were similar to a set of models used for tests reported in NASA Technical Note D-4532; however, the present models have been modified to include longer supporting cables. The accuracy with which each modified membrane achieved the design paraboloidal shape was measured by using an optical-ray-trace technique.

The test results indicated that the larger the metal hub, the better the concentration of incident energy. At the design aperture-diameter ratio for a typical solar Rankine-cycle system with a design geometric efficiency of 0.99, a geometric efficiency of 0.92 was obtained for the modified model with the 0.50 metal-hub radius. When compared with the 0.50 metal-hub-radius model of the earlier investigation, the modified model showed a significant improvement in concentrating ability as evidenced by a reduction in membrane-surface errors. The random errors in both the circumferential and radial directions were reduced by one-half for the modified model. For the three modified models, the largest deviation in apparent focal length was 3 percent less than the design value. The membrane with the 0.50 metal-hub radius came closest to a parabolic cross section. The cable length was found to be an important factor in the design of a whirling-membrane concentrator. The 0.35 and 0.50 metal-hub-radius models compare favorably with other types of expandable solar concentrators and appear to be suitable for low-temperature space power systems.

INTRODUCTION

Solar-energy concentrators used in conjunction with electrical-conversion devices have been considered for space power systems. (For example, see ref. 1.) Expandable

concentrators were of interest for large power systems that required concentrators much larger than launch-vehicle diameters because these concentrators could be compactly packaged for launch and later deployed for use in space. One expandable concentrator that has been proposed employs a whirling membrane (ref. 2) and is also currently of interest for large antennas. For this type of concentrator, a thin aluminized plastic membrane, which has been preformed to an approximate paraboloid and attached to a metal hub, is rotated about its optical axis (axis of symmetry). The centrifugal loading plus an axial component of loading applied at the rim by a conical membrane stretches the approximate paraboloid into the desired paraboloid.

In reference 3, the results of optical-ray-trace tests on three 3.05-m-diameter whirling-membrane models with metal hubs of different diameters are reported. Those results indicate that the best model is efficient when a low concentration of energy is required but is not suitable for systems requiring a very accurate paraboloid to give a high concentration of energy. For the three models, a series of cables replaced the conical membrane which was used in the design configuration of reference 2. The test results of reference 3 also indicate that the concentrating ability of the membrane can be improved significantly by moving the cable hub to a location above the design value on the spin shaft. Based on the results of reference 3, a set of three modified concentrator models was built. These models had different cable lengths and cable-hub locations but the same design values of membrane diameter, metal-hub diameters, focal length, and rim angle as the models of reference 3, hereafter called the original models.

The main objective of the present investigation was to measure the accuracy with which a whirling-membrane concentrator assumes a paraboloidal shape while being rotated. One other objective was to determine the effect of metal-hub size on the formation of circumferential wrinkles in the membrane when optimum cable parameters are used.

Optical-ray-trace tests using a light source and solar cells were conducted to determine the geometric properties of the concentrator models. Data for the three modified models are presented and compared with data for the best concentrator model of reference 3.

SYMBOLS

The units used for the physical quantities defined in this paper are given in the International System of Units (SI). Factors relating this system to U.S. Customary Units are given in reference 4.

A aperture-diameter ratio, ratio of aperture diameter intercepting reflected energy to concentrator diameter

b scattering-circle diameter (see fig. 20)

d paraxial-image diameter, diameter of light-source image formed at focus by cone of rays reflected from paraboloid vertex, $f_d \tan \alpha$

dV element of volume, $R_2\, dR_2 \int \psi\left(R_2,\phi_2\right) d\phi_2$

f_a apparent focal length of concentrator, z_s distance at which the peak of the average irradiance-ratio distribution, as determined from the tests, falls on optical axis

f_d design focal length of concentrator

f_p focal length of geometrically perfect concentrator

i,j,k orthogonal coordinate system with origin at 0'', defining membrane-surface-slope errors where k is the normal to the design paraboloid surface, and j is in a plane containing the optical axis and a membrane radius through 0'' (see figs. 6 and 11)

I_{av} average irradiance ratio, arithmetic average of measured irradiance ratios from five test light-source locations, $\frac{\sum I_m}{5}$

I_{calc} calculated average irradiance ratio in survey plane of a test model, $\frac{1}{2\pi}\int_0^{2\pi} I_{av}(c,\theta)d\theta$, where c is a particular value of r

I_i calculated irradiance ratio in focal plane of a geometrically imperfect and totally illuminated whirling membrane

I_m measured irradiance ratio, ratio of irradiance in survey plane to irradiance incident on test model for one light-source location

I_p calculated irradiance ratio in focal plane of a geometrically perfect and totally illuminated whirling membrane

r,θ plane polar coordinates with origin at 0' in solar-cell survey plane (see fig. 6)

r' radius of cross-sectional area of test light source

r_h metal-hub radius of concentrator

r_o smallest value of r for which $I_{calc} = 0$

R design radius of membrane paraboloid

R_1,ϕ_1 plane polar coordinates with origin at F in focal plane (see fig. 20(b))

R_2,ϕ_2 plane polar coordinates with origin at p in focal plane (see fig. 20(b))

s distance from focal point F to point p in focal plane (see fig. 20(b))

x,y,z rectangular Cartesian coordinates with origin at 0 defining membrane paraboloid (see fig. 6)

x_L light-source position, distance along X-axis from optical axis to center of light source (see fig. 6)

x_d x-ordinate of design membrane

x_m x-ordinate of membrane construction mold

z_c cable-hub position, distance along optical axis from design paraboloid vertex to intersection of extension of cables with optical axis (see fig. 1)

z_d z-ordinate of the design membrane

z_e z-ordinate of the membrane as determined from experiments

z_m z-ordinate of membrane construction mold

z_p z-ordinate of a perfect paraboloid with a focal length of f_a

z_s solar-cell-bar position, distance along optical axis from design paraboloid vertex to survey plane containing solar cells (see fig. 6)

$\Delta x = x_d - x_m$

$\Delta z = z_e - z_d$

$\Delta z' = z_p - z_d$

$\Delta z'' = z_d - z_m$

α collimation angle, angle subtended by light source at concentrator surface (see fig. 19)

$$\beta = \cos^{-1} \frac{\mu^2 + \lambda^2 - \frac{b^2}{4d^2}}{2\mu\lambda}$$

$$\gamma = \frac{\sigma}{d}$$

δ_c circumferential-slope error, projection of angle between actual membrane surface normal and design paraboloid normal in ik-plane (see fig. 11)

δ_r radial-slope error, projection of angle between actual membrane surface normal and design paraboloid normal in jk-plane (see fig. 11)

δ_r' radial-slope difference, angle between the surface normal of a perfect paraboloid with focal length f_a and the design paraboloid normal

η_g geometric efficiency, ratio of energy entering a given-size focal-plane aperture to total energy that is specularly reflected from concentrator

$$\lambda = \frac{s}{d}$$

$$\mu = \frac{R_2}{d}$$

$$\rho = \frac{R_1}{d}$$

σ standard deviation of reflected cone centers as measured from optical axis

σ_c standard deviation of circumferential-slope errors from mean errors

σ_r standard deviation of radial-slope errors from the mean errors

σ_t standard deviation calculated from test data, value of r for which

$$\frac{\int_0^{\sigma_t} I_{calc}(r)dr}{\int_0^{r_o} I_{calc}(r)dr} \approx 0.68$$

ψ Gaussian density function, $\frac{1}{\sqrt{2\pi}\sigma} e^{-\frac{R_1^2}{2\sigma^2}}$ (see fig. 20(a))

MODELS

Configurations

A sketch of the whirling-membrane solar concentrator is shown in figure 1. The concentrator consisted of an aluminized plastic paraboloid, metal hub, shaft, cables, and cable hub. The design paraboloid diameter was 3.05 m, the rim angle was 1.05 rad, and the focal length was 132.1 cm. The membrane was constructed of 0.01-mm-thick aluminized polyethylene-terephthalate plastic and was formed of 45 triangular gores assembled on a convex mold. The gores were attached to each other at a butt joint which was covered with an aluminized plastic strip sealed with a thermosetting resin.

Three models with ratios of metal-hub radius to membrane radius of 0.20, 0.35, and 0.50 were built, and a membrane was fabricated for each model. The convex mold also served as a jig for attaching each membrane to its respective hub in the assembly process. Each model had seventy-two 0.8-mm-diameter steel cables which were attached from the cable hub mounted on the shaft to plastic tabs at the membrane rim. The vertical location of the cable hub on the shaft could be adjusted manually. The design cable-hub locations and cable lengths are shown in table I. Several other cable-hub locations were used during the tests and are shown in table II.

Design Considerations

The equations for the design of a whirling-membrane paraboloid with a conical covering are given in reference 2. These equations were used to calculate the membrane deflections under operating conditions for the models of reference 3 and the present models. However, two changes were made in the deflection calculations for the present

models. First, the deflections were calculated by using an electronic digital computer. Figure 2 shows the deflections $\Delta z''$ and Δx for the original and modified 0.20R hub models. The small difference noted between the two curves is apparently due to the increased number of significant figures used by the digital computer. Second, the deflection equations were modified to include the effects of gravity; however, the results showed that gravity had a negligible effect on the deflections.

As in the investigation of reference 3, cables were used to replace the conical covering, and deflection equations for the conical covering could not be used to determine cable length and cable-hub location on the spin shaft. An approximate solution, which requires an assumed value for the angle between the cables and the membrane-rim plane at the cable-membrane juncture, was used to calculate the cable parameters. The test results of the original models indicated that an assumed value of 1.57 rad for the angle between the cable and rim plane did not result in a very accurate paraboloid. These test results, when considered with those of reference 2, suggest that an angle of 0.52 rad should give a more accurate paraboloid. Therefore, this value was used for the present models, and the resulting cable lengths and cable-hub locations are shown in table I.

As with the original models, the prevention of circumferential wrinkles, which degrade energy concentration, was another important design problem. These wrinkles may form if a suitably large ratio of meridional to circumferential stress is not maintained. One method for preventing wrinkling (discussed in ref. 2) requires increasing the metal-hub radius relative to the membrane radius and thereby increasing the ratio of meridional stress to circumferential stress. Calculated stress ratios, which include and exclude the effects of gravity, are shown in figure 3 for the three hub models. There are only insignificant differences in the two sets of stress ratios. Therefore, hub sizes selected for the present investigation were the same as those used in reference 3.

APPARATUS AND TESTS

The apparatus for testing the concentrators is shown schematically in figure 4, and a photograph of the test arrangement with the 0.35R metal-hub model rotating at 71 rad/s is shown in figure 5. The optical-ray-trace equipment consisted of a light source to give a nearly collimated beam of light and 10 silicon solar cells to measure the reflected light distribution in the focal region. An additional solar cell in the light-source tube continuously monitored the incident irradiance.

All tests were made in a vacuum sphere at pressures below 133 N/m^2 (1 mm of mercury). All models were tested at the design rotational speed of 71 rad/s. Table II gives the light-source and solar-cell-bar locations in addition to the various model

configurations. Figure 6 shows the coordinate systems relating the locations of the whirling membrane, light source, and solar cells.

Each model was tested at its design cable-hub location and at various locations above the design value; however, for the 0.20R hub model, the test at the design location was not completed because of a cable failure. Data for each model configuration were obtained by placing the solar-cell bar at a vertical location in or near the design focal plane, positioning the light source, and then surveying the plane by rotating and moving the solar-cell bar. In order to obtain data representative of different areas of the membrane, the light source was positioned at five different radial locations. A more detailed description of the apparatus and test procedures can be found in reference 3.

REDUCTION AND ACCURACY OF DATA

The basic data measured during the investigation were solar-cell voltages. The voltage readings from each solar cell on the bar were divided by the monitor-cell voltage, recorded over the same time interval, to eliminate the effect of change in the test light-source irradiance. The resulting voltage ratios were adjusted by using solar-cell calibration factors obtained from laboratory tests in order to put the data on a common basis. The adjusted voltage ratio, defined as irradiance ratio I_m, represents the factor by which the irradiance of the incident energy has been modified by concentrator geometry and specular reflectance of the aluminized plastic.

Several sources of error in the magnitude and location of the irradiance-ratio data existed in the test arrangement. The solar-cell calibration factors are considered to be accurate within ±10 percent. The alinement of the light source parallel to the concentrator optical axis was made within ±1.7 mrad, which represents a focal-plane image displacement that varies from 3 mm for the innermost light-source location to 5 mm for the outermost location. The location of the solar cells on the bar was determined to be within 0.4 mm of the nominal 2.5-cm intervals. The axis of rotation of the bar was within 0.4 mm of the axis of rotation of the concentrator, the angular location of the bar was within ±0.04 rad of the desired location, and the vertical location of the bar was within 0.8 mm of the desired location. The misalinement of the light source and the displacements of the solar cells from their nominal locations are not readily transferable to a percentage error in irradiance ratio; however, the irradiance-ratio error involved is considered to have a minor effect on the overall accuracy of the data.

RESULTS AND DISCUSSION

Concentrator Geometric Efficiency

The determination of the accuracy with which the whirling-membrane concentrator assumes the design paraboloid was the primary test objective. One measure of the concentrator accuracy is geometric efficiency. The cable-hub location which optimized geometric efficiency was located first and is included in the range of test parameters for each model in table II. Irradiance-ratio distributions along the $\theta = 0^{o}$-180^{o} and $\theta = 90^{o}$-270^{o} axes for the optimum configurations of each model are shown in figure 7. (These distributions are typical of those obtained with the other model configurations.) To obtain the geometric efficiency for the entire concentrator, the irradiance-ratio values for the five light-source locations were averaged. The resulting average distributions (fig. 8) were used, as discussed in reference 3, to calculate the geometric efficiencies of the three models.

Figure 9 presents the geometric efficiency for the optimum configuration of each model and for a perfect paraboloid of the same diameter and focal length as the whirling membrane. The data indicate that the larger the hub, the better the geometric efficiency. Aperture-diameter ratios A for the best test model are generally two orders of magnitude larger than ratios for the perfect paraboloid and thereby indicate that even the best test model is only an approximate paraboloid. (The aperture-diameter ratio is the ratio of the aperture diameter intercepting reflected energy in the focal plane to the concentrator diameter.)

The comparison of figure 9, however, is based on results obtained by using a test light source; whereas in a space power system, the whirling membrane would be illuminated by the sun. Therefore, the effect of solar illumination on the concentrating ability of the optimum configuration of the 0.50R hub model was examined, and the results are given in the appendix. As shown in the appendix, the effect on geometric efficiency is minor when the membrane illumination is changed from the test light source to the sun; therefore, the test-model efficiency curves shown in figure 9 are good indications of solar geometric efficiency. The efficiency curve for a perfect paraboloid illuminated by the sun is also shown for comparison with the test data. As can be seen, the test data more closely approach the geometric efficiency for a perfect paraboloid when application of the whirling membrane as a solar concentrator is considered.

The geometric efficiencies of the 0.35R and 0.50R hub models and of two other expandable concentrators that use thin reflective membranes are shown in figure 10 for comparison. The data for the inflatable-rigidized and split-rib-umbrella concentrators (refs. 5 and 6, respectively) were obtained from solar calorimetric tests. The whirling-membrane concentrator with either the 0.35R or 0.50R metal hub, in its present form,

appears competitive with other expandable concentrators for use in relatively low temperature, space power systems.

Concentrator Geometry

As noted earlier, all models were only approximate paraboloids. An examination of figure 7 suggests that two types of errors, mean and random, were present in the surfaces. The mean errors are evidenced by the displacement, from the optical axis, of the peaks of the irradiance-ratio distributions. The mean error consists of a combination of displacement in the z direction of the actual surface from the design paraboloid and an angle between the normal to the actual surface and the normal to the design paraboloid. The local coordinate system for the surface normals is shown in figure 6; the radial and circumferential projections of the slope error δ_r and δ_c, respectively, are shown in figure 11.

The vertical displacements Δz and the radial-slope errors δ_r were determined for the configurations with optimum cable-hub locations and are shown in figure 12. The membranes for the three models appear to have lifted above the design ordinates and the slope for the 0.35R and 0.50R hub models increased. Although the membranes for the optimum configuration of each model did not attain the design parabolic cross section, the membranes did achieve approximate parabolic cross sections with apparent focal lengths f_a shorter than the design value of 132.1 cm. The 0.20R, 0.35R, and 0.50R hub models had apparent focal lengths of 130.8, 129.1, and 128.6 cm, respectively, as shown in figure 8. The ordinate and slope differences between perfect paraboloids with the apparent focal lengths and the design paraboloid were calculated and are shown in figure 12 for comparison with the test data. Comparison shows that only the 0.50R hub model had a membrane shape very close to that of a perfect paraboloid with the same focal length.

In contrast to the irradiance-ratio distributions along the $\theta = 0^\circ\text{-}180^\circ$ axis, the peak values of the distributions along the $\theta = 90^\circ\text{-}270^\circ$ axis occur, for the most part, on the optical axis as can be seen in figure 7. Therefore, there is no indication of mean errors in the circumferential direction for any of the models, and the membranes on the average were surfaces of revolution.

Random errors existed in all model configurations as evidenced by relatively wide irradiance-ratio distributions compared with distributions for a perfect paraboloid. For example, some of the distributions along the $\theta = 0^\circ\text{-}180^\circ$ axis in figure 7 have nonzero values more than 20 cm on either side of the peak values; whereas for a perfect paraboloid, the nonzero values would have been within 1 mm from the peak values. The shapes of the distributions are similar to normal probability curves. The standard deviation of the radial-slope errors σ_r for the optimum configuration of each model is shown in

figure 13(a). It can be seen that the larger the metal hub, the smaller the standard deviation. This standard deviation probably results from the scattering of the incident light by circumferential wrinkles in the membrane. Therefore, the behavior shown in figure 13(a) tends to confirm the analysis of reference 2 which indicates that for a larger metal hub there will be a higher ratio of meridional to circumferential stress in the membrane and, consequently, less circumferential wrinkling. Standard deviations of the circumferential-slope errors σ_c could be determined only at a few membrane radii for the three models. As shown in figure 13(b), values of σ_c, like those of σ_r, decrease with increasing metal-hub size. Comparison of figure 13(b) with figure 13(a) shows that values of σ_c for each model are approximately one-half the σ_r values at the same membrane radius. Therefore, σ_c is not as important as σ_r in determining the distribution of the reflected energy or the concentrator geometric efficiency.

Effect of Cable-Hub Location

The investigation of reference 3 established that the location of the cable hub relative to the metal hub is an important factor in the design of a whirling-membrane concentrator. Therefore, cable-hub location was varied for the three models in the present investigation, and some of the resulting average irradiance-ratio distributions along the $\theta = 0^{\circ}$-180° axis are shown in figure 14. In general, the figure shows that raising the cable hub above the design values resulted in narrower distributions with higher peak values for the two smaller hub models. Apparently, the higher cable-hub locations resulted in a reduction of the circumferential wrinkling in the membrane; however, the membrane cross sections obtained were not the design geometry. The largest hub model was the best concentrator at the design cable-hub location. At this condition, a parabolic cross section was obtained with a focal length 3.5 cm shorter than the design focal length (132.1 cm). The failure of any membrane to achieve the design shape may be due to the assumptions made in calculating cable-hub location and cable length. However, the assumption that the conical membrane can be replaced by cables may also be a contributing factor.

Comparison of Modified 0.50R Hub Model With Original 0.50R Hub Model

As with the original models (ref. 3), the 0.50R hub model of the present investigation gave the best concentration of energy. Therefore, the optimum configurations of the original and modified 0.50R hub models are compared in order to indicate the improvements obtained as a result of the modifications.

Figure 15 shows the average irradiance-ratio distributions along the $\theta = 0^{\circ}$-180° and $\theta = 90^{\circ}$-270° axes for both the original and modified models. The modified model has much narrower distributions with a threefold increase in the peak value compared

with the original model. These narrower distributions result in a more efficient concentrator as shown in figure 16. Also shown in figure 16 is the design geometric efficiency for a typical solar Rankine-cycle system (ref. 7). The original model had an efficiency of only 0.58 at the design aperture-diameter ratio, whereas the modified model has an efficiency of 0.92, which is only about 0.07 below the design value.

The membrane-surface errors for the original and modified models are shown in figures 17 and 18. The membrane vertical displacements from the design paraboloid are shown in figure 17. Both models had a design focal length of 132.1 cm; whereas apparent focal lengths f_a of 130.6 and 128.6 cm were obtained for the original and modified models, respectively. When compared with perfect paraboloids with these focal lengths, as shown in figure 17, the modified model has attained a shape more nearly that of a paraboloid. As shown in figure 18, the random radial-slope error for the modified model was about one-half that for the original model over the survey radius. This difference indicates that the modified model probably experienced significantly less circumferential wrinkling than the original model. The decrease in the random radial-slope error for the modified model was also accompanied by a corresponding decrease in the random circumferential error.

The improvements in the modified model can be considered to be related to the longer cables. Differences in design ordinates between the two models were too minor to account for much of the differences in membrane contour, and cable-hub locations were essentially the same.

CONCLUSIONS

Three 3.05-m-diameter whirling-membrane concentrators similar to models tested previously have been investigated by the measurement of the accuracy with which the models focus incident energy. The three models had metal hubs with ratios of hub radius to membrane radius of 0.20, 0.35, and 0.50. The test results for the modified models indicate the following:

1. The larger the metal hub, the better is the concentration of incident energy. The modified model with the 0.50 metal-hub radius gave the best concentration and had the following properties:

(a) The membrane was approximately parabolic with an apparent focal length of 128.6 cm, which is about 3 percent less than the design value of 132.1 cm.

(b) At the design aperture-diameter ratio for a typical solar Rankine-cycle system with a design geometric efficiency of 0.99, a geometric efficiency of 0.92 was obtained.

(c) There was significant improvement in concentrating ability when compared with the original model with a 0.50 metal-hub radius. For example, the random errors in the membrane in both the circumferential and radial directions were reduced by one-half for the modified model.

2. The cable length and the location of the cable hub relative to the metal hub are important factors in the design of a whirling-membrane concentrator.

3. The whirling-membrane concentrator with the 0.35 or 0.50 metal-hub radius compares favorably with other types of expandable solar concentrators and appears to be suitable for low-temperature space power systems.

Langley Research Center,
National Aeronautics and Space Administration,
Hampton, Va., April 10, 1970.

APPENDIX

EFFECT OF SOLAR ILLUMINATION ON WHIRLING-MEMBRANE PERFORMANCE

The whirling membrane has been proposed as a solar-energy concentrator. The models of the present investigation were tested with a light source having a collimation angle of 0.66 mrad as compared with a collimation angle of 9.3 mrad for the sun. The collimation angle is the angle subtended by the light source at a point on the concentrator surface and is illustrated in figure 19 for the case of solar illumination. The collimation angle can have a large effect on the peak value and distribution of the energy reflected by a geometrically perfect paraboloid. However, for a concentrator with surface errors, such as the whirling-membrane test models, the effect of collimation angle can be much less. For example, in reference 3, it was noted that the geometric efficiencies calculated for the test models were, for large aperture sizes, approximately the same as those for solar illumination. In order to obtain a better estimate of the effect of solar illumination on the whirling-membrane performance, the method of reference 8 has been modified and used to calculate focal-plane energy distributions for various collimation angles.

As shown in figure 19, the solar radiation reflected from a concentrator is contained in cones defining the solar collimation angle. It was assumed in reference 8 that for a geometrically imperfect concentrator, the reflected cone centers are distributed uniformly within a "scattering circle" in the focal plane. However, figure 7 shows that the whirling-membrane test data have approximately Gaussian distributions. Since the test-data distributions are very wide compared with the paraxial-image diameter (0.09 cm), the distribution of reflected cone centers for the test models have, therefore, been assumed to be Gaussian.

Figure 20 shows a typical Gaussian distribution of reflected cone centers in the focal plane of a geometrically imperfect concentrator. The Gaussian distribution may be represented by

$$\psi(R_1) = \frac{1}{\sqrt{2\pi}\sigma} e^{-\frac{R_1^2}{2\sigma^2}} \tag{1}$$

where σ is the standard deviation of reflected cone centers as measured from the optical axis. It is assumed that most of the reflected cone centers fall within the scattering circle so that $\psi(R_1) \approx 0$ for $R_1 \geq \frac{b}{2}$. Neglecting the relatively few cone centers outside the scattering circle will have a minor effect on the calculated energy distributions.

APPENDIX

The irradiance ratio I_i at a point p shown in figure 20(b) is determined by –

(1) Calculating the fraction of cone centers occurring in an annulus of differential width dR_2 at a distance R_2 from p

(2) Multiplying this fraction of cone centers by the irradiance ratio I_p at a distance R_2 from the focal point of a geometrically perfect whirling membrane

(3) Integrating these products over suitable limits of R_2

The fraction of cone centers in the differential annulus is obtained by calculating the ratio of the differential volume $dV(R_2,\phi_2)$ bounded by the annulus and $\psi(R_1)$ to the total volume bounded by $\psi(R_1)$ and the scattering circle. The general form of the differential volume is

$$dV(R_2,\phi_2) = R_2\, dR_2 \int \psi(R_2,\phi_2)d\phi_2 \tag{2}$$

The total volume enclosed by the Gaussian distribution and the scattering circle is given by

$$\int_0^{b/2}\int_0^{2\pi} \psi(R_1)\, R_1\, d\phi_1\, dR_1 \approx \sqrt{2\pi}\sigma \tag{3}$$

By using equations (2) and (3), the irradiance ratio I_i at p may be written as

$$I_i(s) = \frac{1}{\sigma\sqrt{2\pi}} \iint I_p(R_2)\, \psi(R_2,\phi_2)\, R_2\, dR_2\, d\phi_2 \tag{4}$$

By rewriting equations (1) to (4) in terms of the nondimensional variables γ, λ, μ, and ρ, where $\gamma = \frac{\sigma}{d}$, $\lambda = \frac{s}{d}$, $\mu = \frac{R_2}{d}$, and $\rho = \frac{R_1}{d}$, the irradiance ratio at p becomes

$$I_i(\lambda) = \frac{1}{\gamma\sqrt{2\pi}} \iint I_p(\mu)\, \psi(\mu,\phi_2)\, \mu\, d\mu\, d\phi_2 \tag{5}$$

Values for I_p are dependent on collimation angle and can be found in reference 8.

Equation (5) was evaluated for various regions in the focal plane, and the following results were obtained:

For $\lambda \geq \frac{b}{2d}$ and $\frac{b}{d} > 0$ (p outside or on the scattering circle),

APPENDIX

$$I_i(\lambda) = \frac{1}{\pi\gamma^2}\int_{\lambda-\frac{b}{2d}}^{\sqrt{\lambda^2-\left(\frac{b}{2d}\right)^2}} I_p(\mu)\int_0^{\beta} e^{-\frac{\rho^2}{2\gamma^2}}\, d\phi_2\mu\, d\mu + \frac{1}{\pi\gamma^2}\int_{\sqrt{\lambda^2-\left(\frac{b}{2d}\right)^2}}^{\lambda+\frac{b}{2d}} I_p(\mu)\int_0^{\beta} e^{-\frac{\rho^2}{2\gamma^2}}\, d\phi_2\mu\, d\mu \tag{6}$$

For $0 < \lambda \leqq \frac{b}{2d}$ and $\frac{b}{d} > 0$ (p inside or on the scattering circle),

$$I_i(\lambda) = \frac{1}{\pi\gamma^2}\int_0^{\frac{b}{2d}-\lambda} I_p(\mu)\int_0^{\pi} e^{-\frac{\rho^2}{2\gamma^2}}\, d\phi_2\mu\, d\mu + \frac{1}{\pi\gamma^2}\int_{\frac{b}{2d}-\lambda}^{\lambda+\frac{b}{2d}} I_p(\mu)\int_0^{\beta} e^{-\frac{\rho^2}{2\gamma^2}}\, d\phi_2\mu\, d\mu \tag{7}$$

For $0 \leqq \lambda \leqq \left(\frac{1}{2} - \frac{b}{2d}\right)$ and $\frac{b}{d} \leqq 1$,

$$I_i(\lambda) = I_i(\lambda = 0) \tag{8}$$

For $\lambda = 0$ and $\frac{b}{d} \geqq 1$,

$$I_i = \frac{1}{\gamma^2}\int_0^{b/2d} I_p(\mu) e^{-\frac{\mu^2}{2\gamma^2}}\, \mu\, d\mu \tag{9}$$

In equations (6) to (9)

$$\beta = \cos^{-1}\frac{\mu^2 + \lambda^2 - \frac{b^2}{4d^2}}{2\mu\lambda} \tag{10}$$

and

$$\rho^2 = \mu^2 + \lambda^2 - 2\mu\lambda\cos\phi_2 \tag{11}$$

These equations have been used to generate focal-plane distributions for the whirling membrane illuminated by the test light source and by the sun. (See fig. 21.) The expression for I_i has been modified by the factor $(r')^2/\left(R^2 - r_h^2\right)$ for comparison with the calculated average irradiance ratio I_{calc} obtained from the test data of the optimum configuration of the 0.50R hub model (figs. 7(e) and 7(f)). A standard deviation σ of 1.25 cm and a scattering-circle diameter b of 22.9 cm were obtained from this

calculated average irradiance ratio I_{calc} where it was assumed that $\sigma_t = \sigma$. Comparison of the calculated irradiance-ratio values I_i for the sun and test light source indicates that increased collimation angle results in a lower peak value and a wider distribution as would be expected. The differences between the I_{calc} and I_i curves for the test light source are attributed primarily to the approximate Gaussian distribution of the test data.

Although the method for calculating the irradiance-ratio distributions I_i does not exactly reproduce the magnitude and shape of the test distribution I_{calc}, the method is considered to give a good representation of the effects of change in collimation angle α. Distributions have been calculated over the range of collimation angles from values for the test light source to those for the sun, and the peak values are shown in figure 22. For comparison, the effect of collimation angle on the calculated peak value for a geometrically perfect concentrator is also shown. The peak value for the perfect concentrator varies approximately as $1/\alpha^2$ with a value of about 4500 for test-light illumination and a value of 23 for solar illumination. This variation contrasts sharply with that for the imperfect concentrator which has a value of 3.5 for the test light source and 3.1 for the sun.

Since the object of these calculations is to show the effect of collimation angle on the performance of concentrators with surface errors, the calculated distributions of figure 21 have been used to determine geometric efficiencies. These geometric efficiencies for test-light and solar illumination are shown in figure 23. The effect of solar illumination is minor and results in only a slight shift of efficiency values to higher aperture-diameter ratios.

REFERENCES

1. Heath, Atwood R., Jr.; and Hoffman, Edward L.: Review of Solar Concentrator Technology. Intersociety Energy Conversion Engineering Conference, Amer. Inst. Aeronaut. Astronaut., Sept. 1966, pp. 231-237.

2. Simmonds, James G.: The General Equations of Equilibrium of Rotationally Symmetric Membranes and Some Static Solutions for Uniform Centrifugal Loading. NASA TN D-816, 1961.

3. Jerke, John M.; and Heath, Atwood R., Jr.: The Geometric Properties of an Expandable Whirling-Membrane Solar-Energy Concentrator. NASA TN D-4532, 1968.

4. Comm. on Metric Pract.: ASTM Metric Practice Guide. NBS Handbook 102, U.S. Dep. Com., Mar. 10, 1967.

5. Rhodes, Marvin D.: Calorimetric Evaluation of Three 1.5-Meter-Diameter Inflatable Rigidized Solar Concentrators. NASA TN D-5234, 1969.

6. Camp, John D.; and Nowlin, William D.: Investigation of the Calorimetric Efficiency of a Split-Rib Umbrella-Type Paraboloidal Solar Energy Concentrator. NASA TN D-2015, 1964.

7. Anon.: Sunflower Solar Collector. NASA CR-46, 1964.

8. Hukuo, Nobuhei; and Mii, Hisao: Design Problems of a Solar Furnace. J. Solar Energy Sci. Eng., vol. 1, no. 2-3, Apr.-July 1957, pp. 108-114.

TABLE I.- DESIGN CABLE PARAMETERS

Metal-hub ratio, r_h/R	Cable length, cm	Cable-hub location, z_c, cm	Cable length, cm	Cable-hub location, z_c, cm
	Original models		Modified models	
0.20	152.4	40.8	152.5	43.1
.35	152.4	40.8	152.9	44.8
.50	152.4	40.8	154.2	50.9

TABLE II.- MODELS AND TEST PARAMETERS

Models			Test parameters								
			Light-source location, x_L, cm					Solar-cell-bar positions			
								Axial position, z_S, cm			Angular position, θ, deg (*)
Configuration	Metal-hub radius, r_h/R	Cable-hub location, z_c, cm									
I-A	0.20	45.6	52.1	86.6	109.7	128.6	141.7	-----	-----	132.1	0° to 315°
I-B		50.7						-----	-----	132.1	
I-C		53.2						-----	-----	132.1	
I-D		55.7						-----	130.8	132.1	
I-E		57.0						-----	131.6	132.1	
I-F		58.2						-----	128.4	132.1	
II-A	.35	44.8	68.3	93.9	113.7	130.5	141.9	-----	129.7	132.1	
II-B		47.3						-----	-----	128.3	
II-C		49.8						-----	129.7	132.1	
II-D		51.1						-----	129.6	132.1	
II-E		52.3						-----	129.1	132.1	
II-F		52.9						-----	-----	129.1	
II-G		53.6						-----	129.6	132.1	
II-H		54.8						-----	-----	132.1	
III-A	.50	50.9	86.3	104.9	120.4	134.1	144.3	128.3	132.1	133.4	
III-B		53.4						-----	-----	133.4	
III-C		54.7						-----	-----	133.4	
III-D		55.3						-----	128.2	132.1	
III-E		55.9						-----	-----	133.4	

*In 45° increments; however, for 0.20R hub model, $\theta = 180°$ could not be taken.

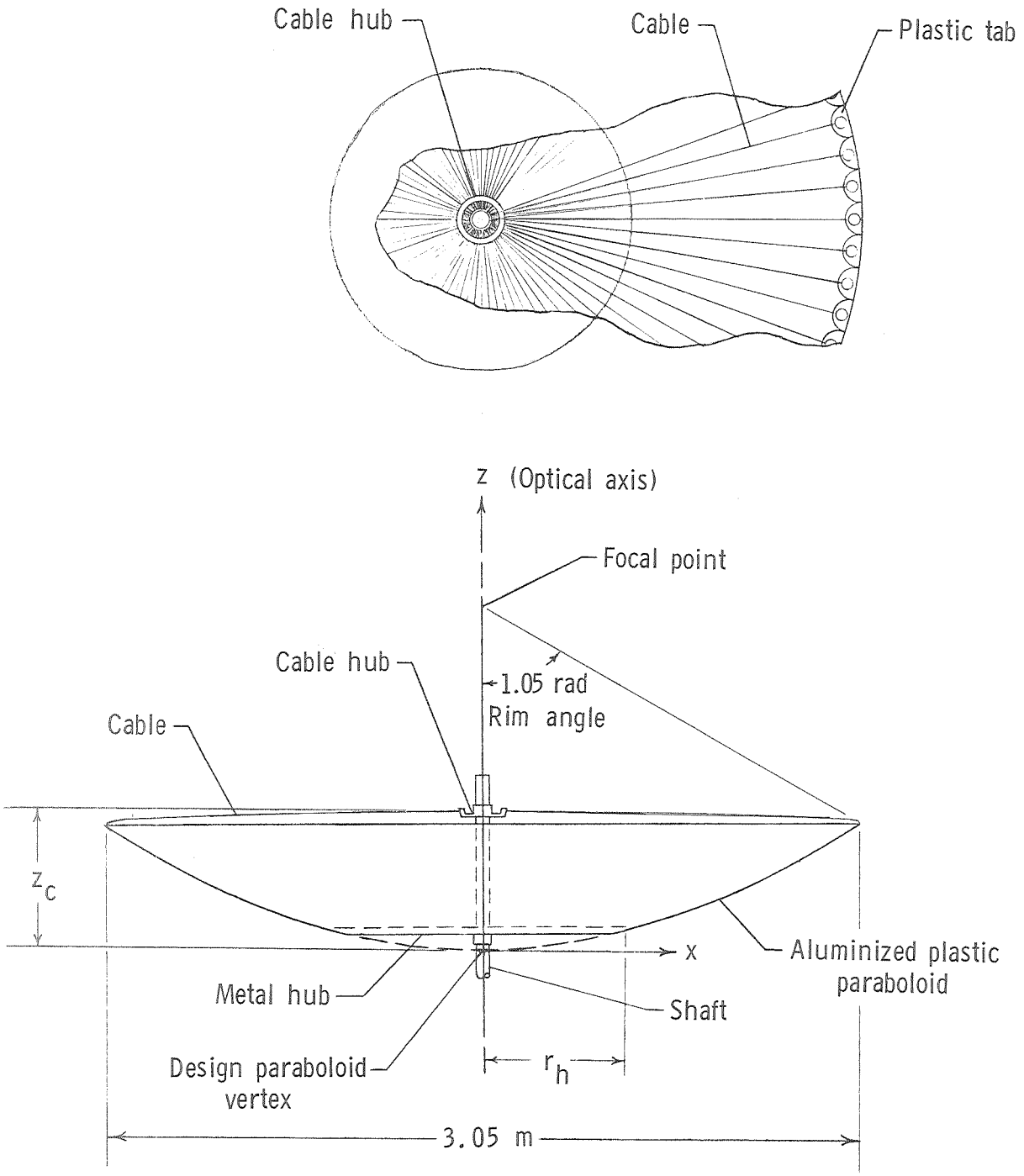

Figure 1.- Sketch of whirling-membrane solar concentrator with design dimensions.

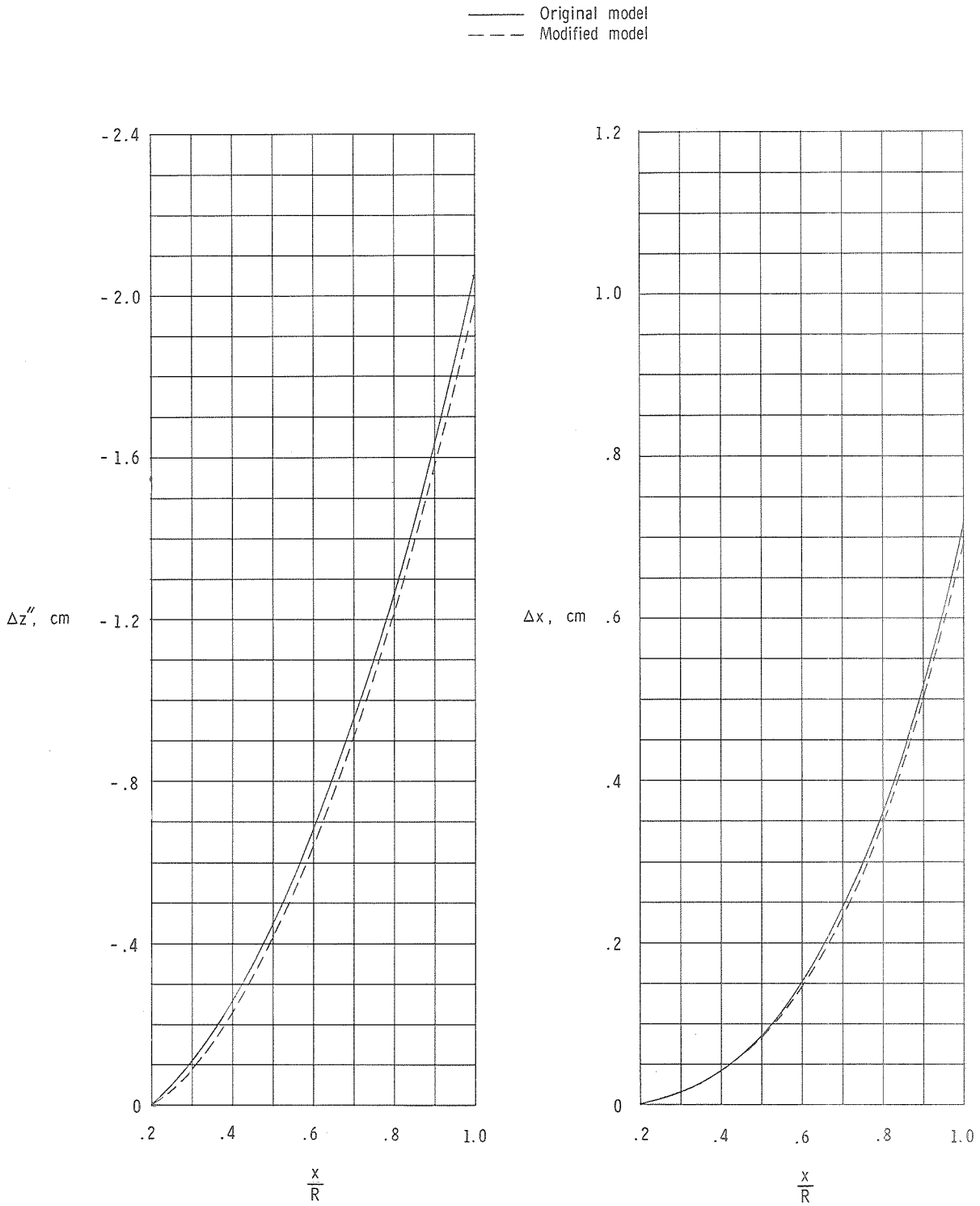

(a) Deflection in z direction.

(b) Deflection in x direction.

Figure 2.- Membrane deflection of 0.20R hub model at design rotational velocity of 71 rad/s.

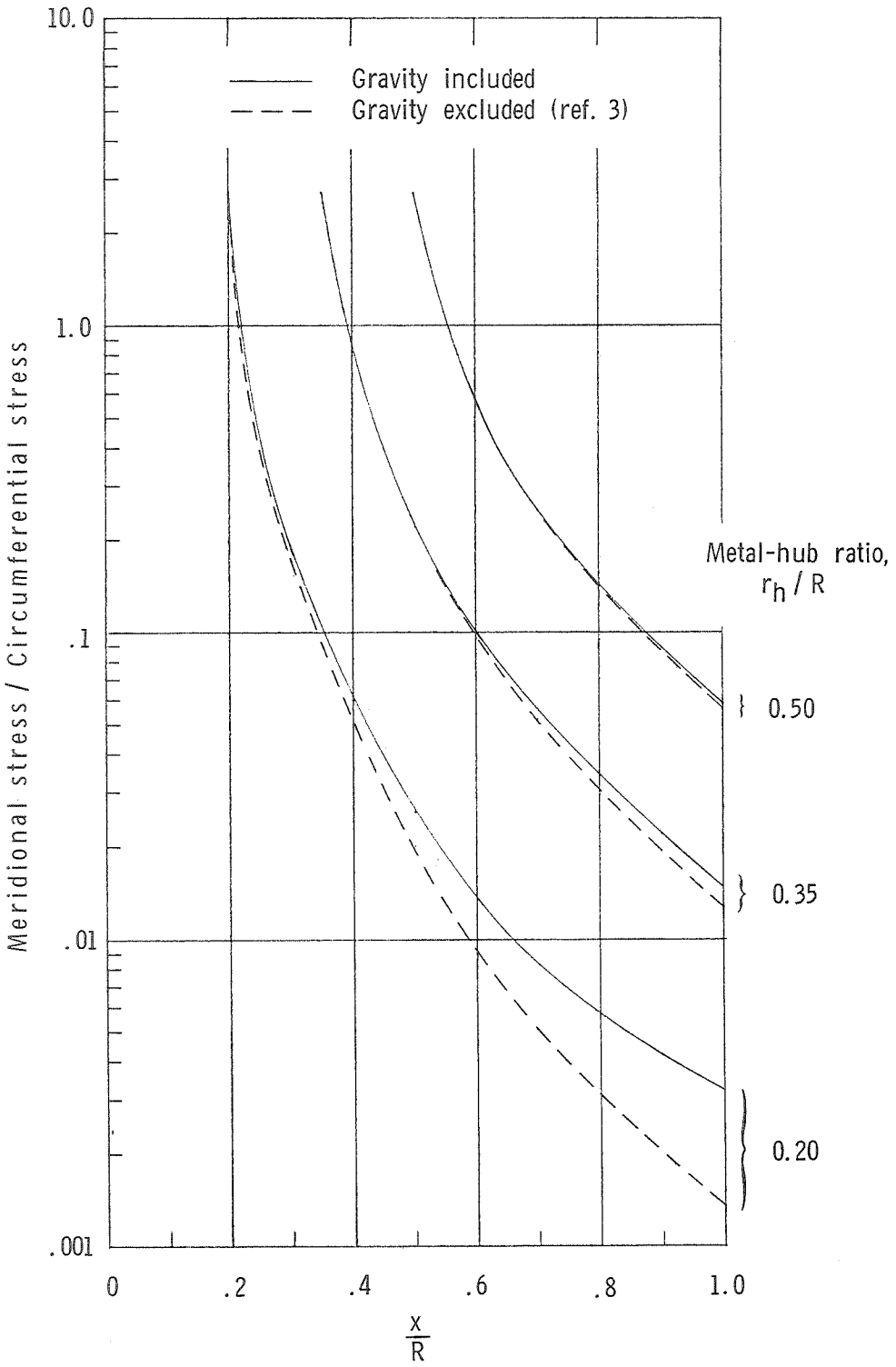

Figure 3.- Variation of stress ratio in the 3.05-m-diameter whirling-membrane concentrator rotating at 71 rad/s.

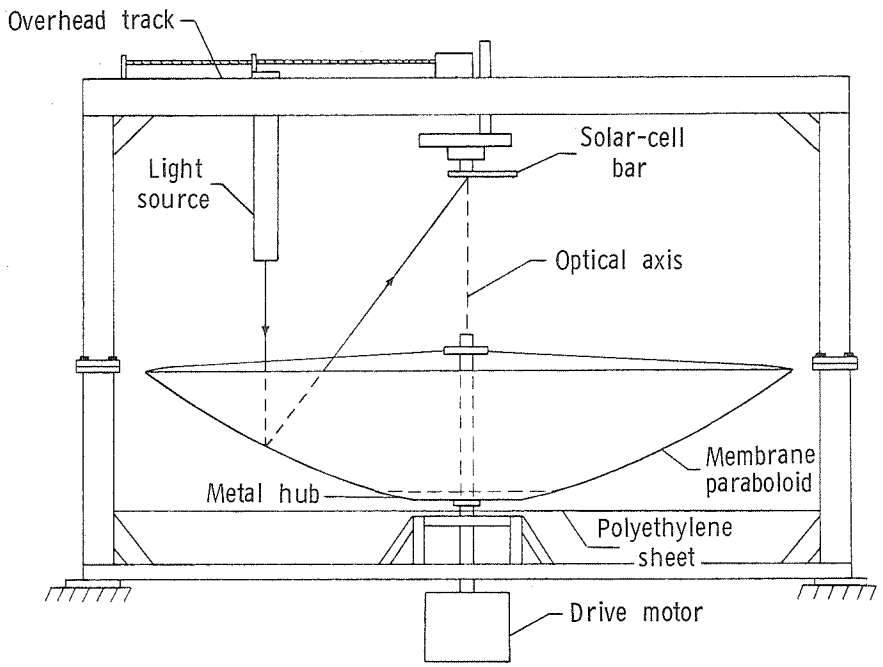

Figure 4.- Schematic of test apparatus.

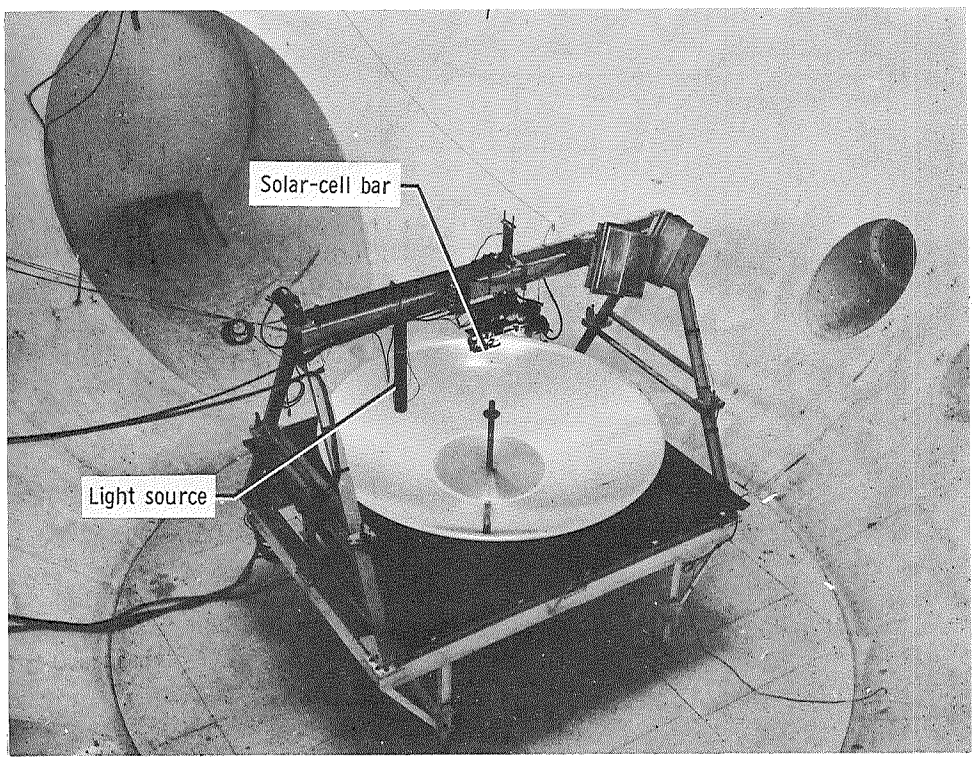

L-66-1824

Figure 5.- Whirling-membrane-concentrator test apparatus, with the 0.35R hub model rotating at 71 rad/s, in the vacuum sphere.

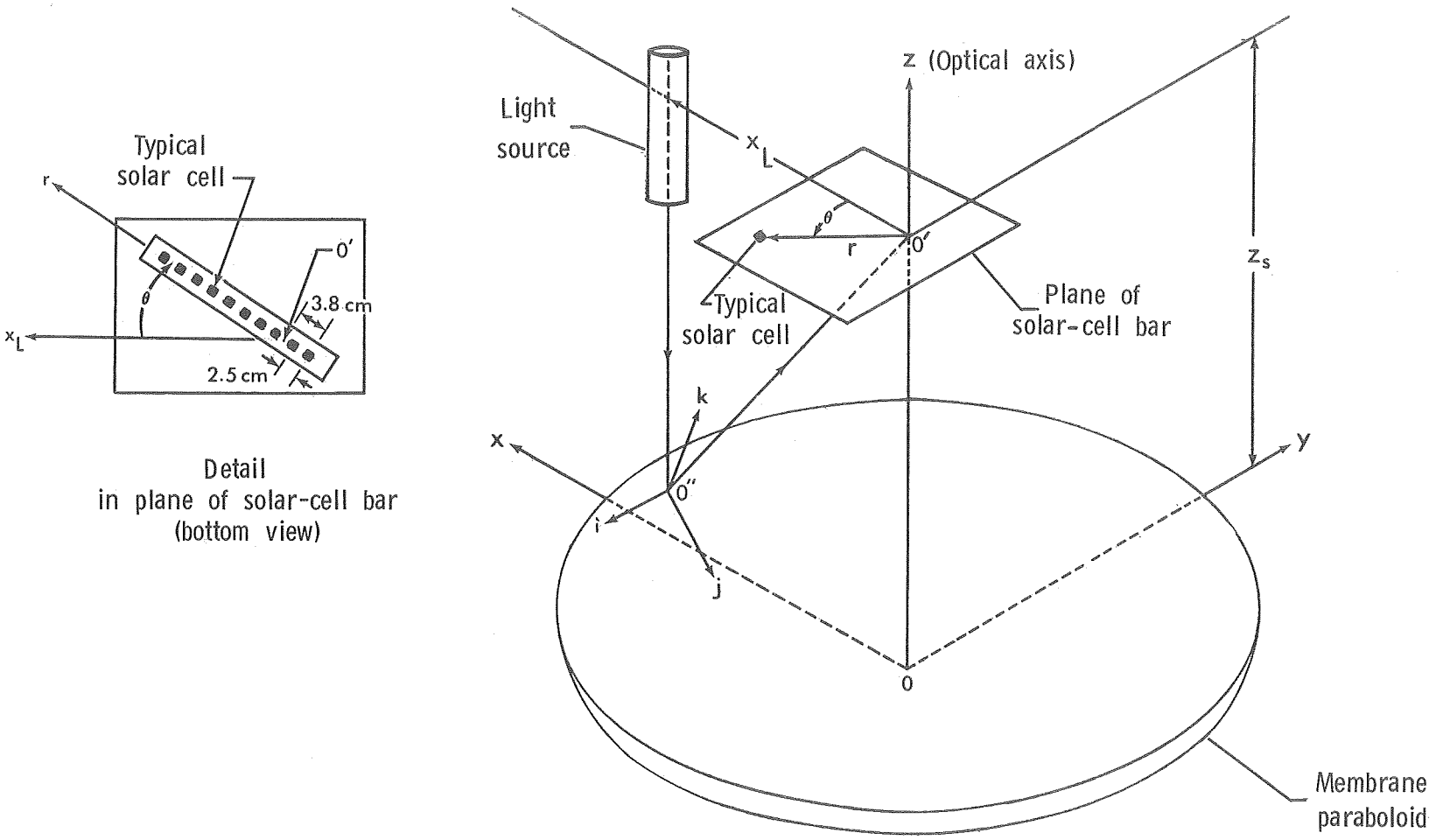

Figure 6.- Coordinate systems relating the locations of the whirling membrane, light source, and solar cells.

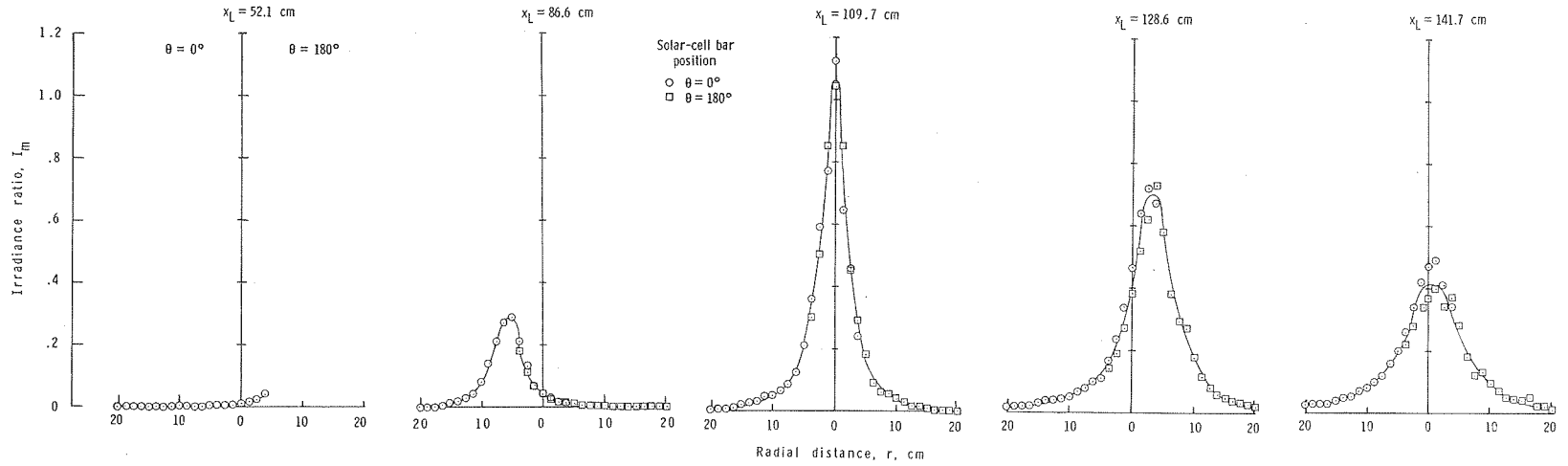

(a) 0.20R hub model (configuration I-D); z_s = 130.8 cm; θ = 0°-180° axis.

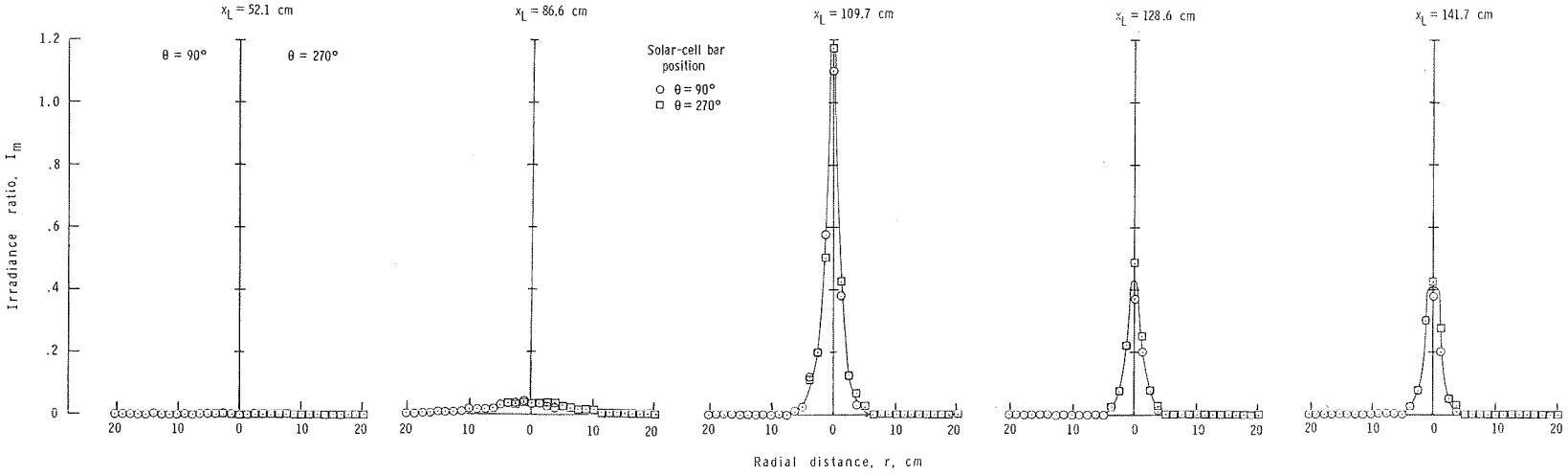

(b) 0.20R hub model (configuration I-D); z_s = 130.8 cm; θ = 90°-270° axis.

Figure 7.- Irradiance-rate distributions along the θ = 0°-180° and θ = 90°-270° axes for the five light-source locations and for the optimum configurations of the three hub models.

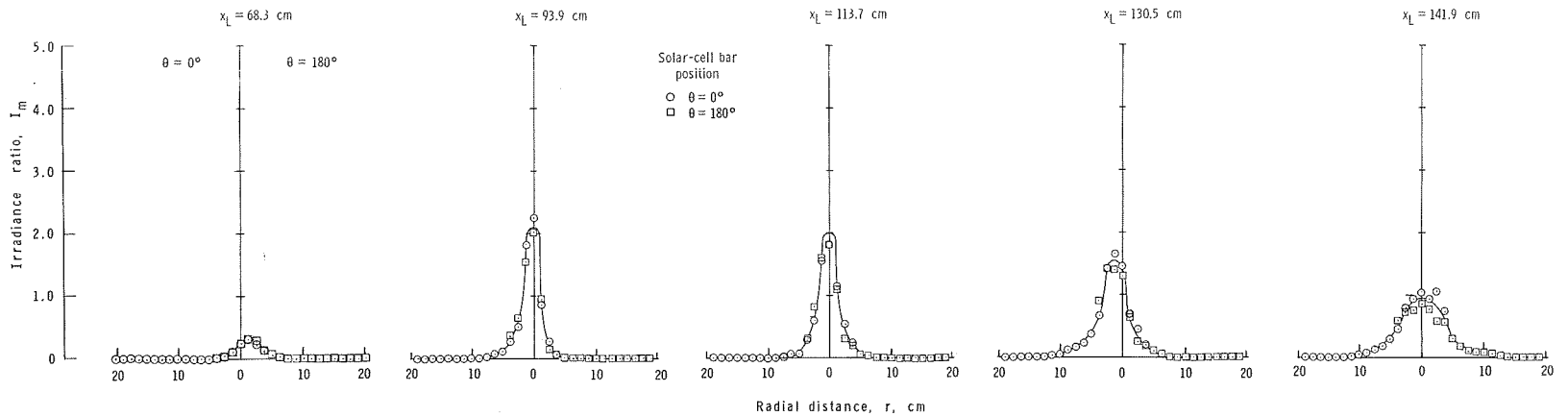

(c) 0.35R hub model (configuration II-F); z_s = 129.1 cm; θ = 0°-180° axis.

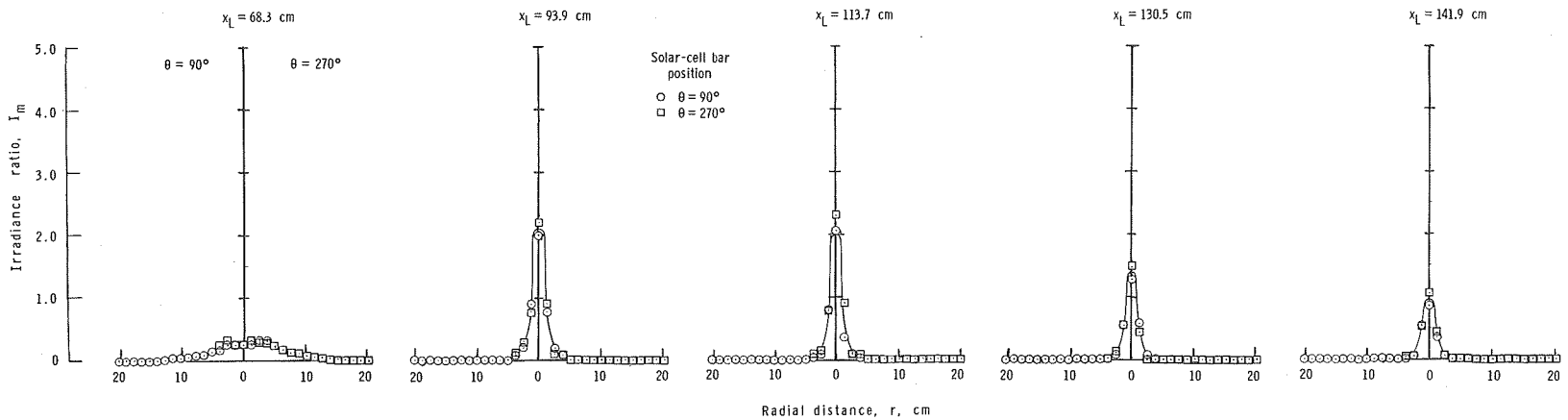

(d) 0.35R hub model (configuration II-F); z_s = 129.1 cm; θ = 90°-270° axis.

Figure 7.- Continued.

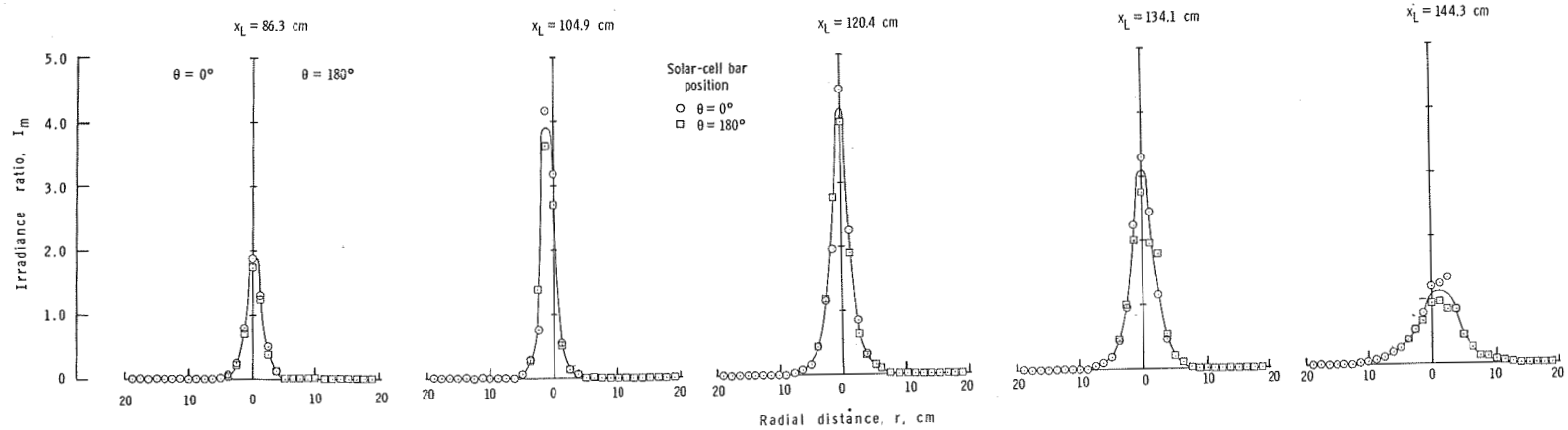

(e) 0.50R hub model (configuration III-A); z_S = 128.3 cm; θ = 0°-180° axis.

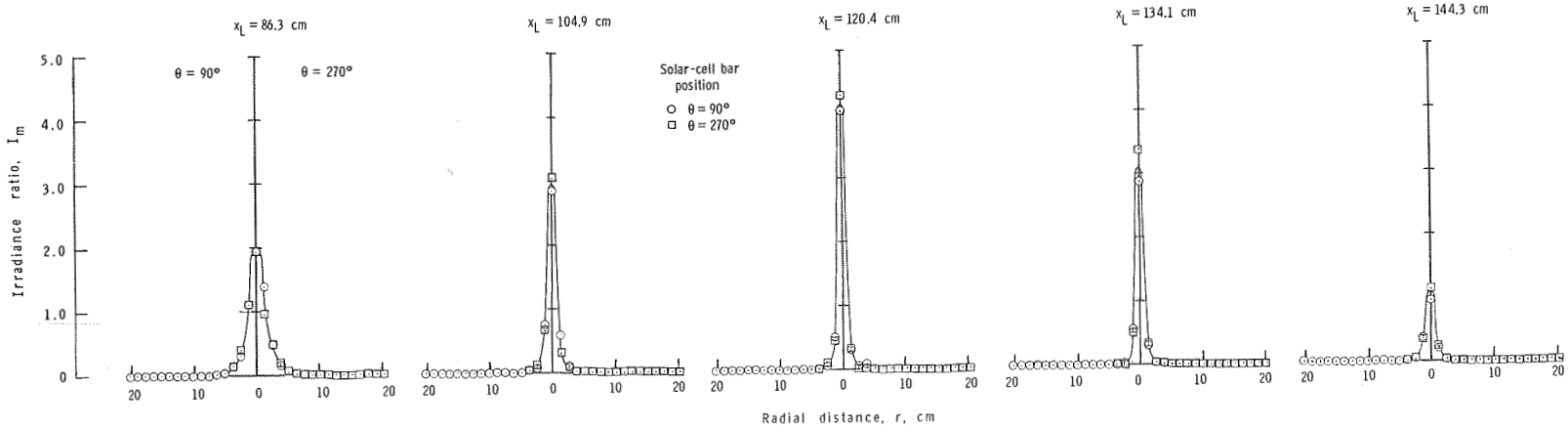

(f) 0.50R hub model (configuration III-A); z_S = 128.3 cm; θ = 90°-270° axis.

Figure 7.- Concluded.

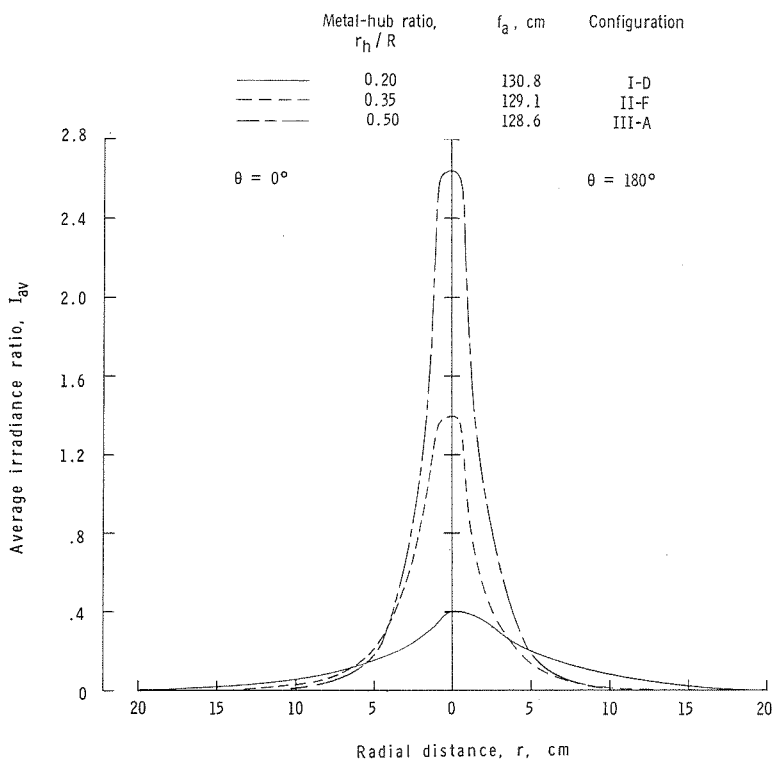

(a) θ = 0°-180° axis.

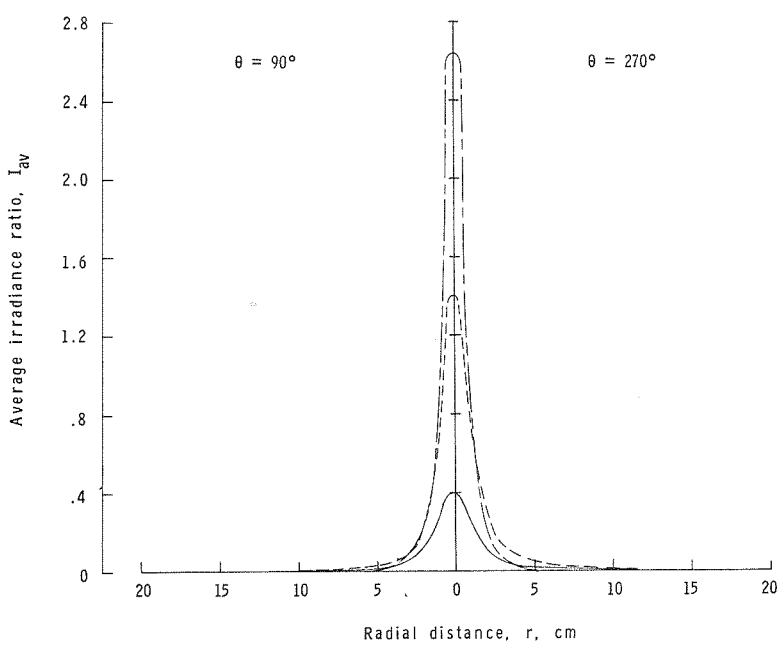

(b) θ = 90°-270° axis.

Figure 8.- Average irradiance-ratio distributions along θ = 0°-180° and θ = 90°-270° axes in the apparent focal planes of the three hub models.

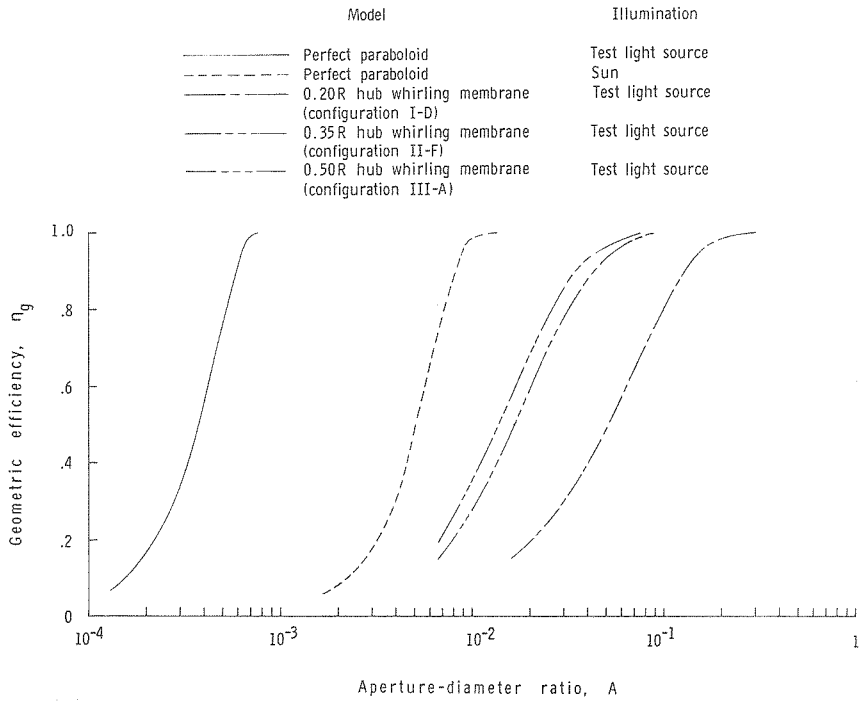

Figure 9.- Geometric efficiency over a range of aperture-diameter ratio.

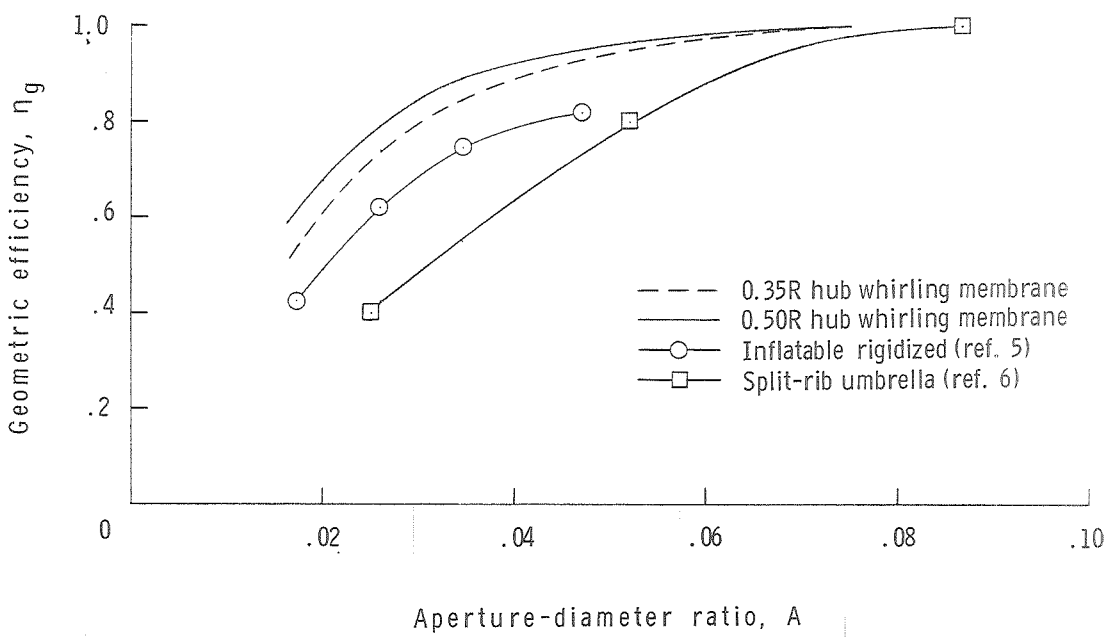

Figure 10.- Geometric efficiencies of two whirling-membrane models and two other expandable concentrators.

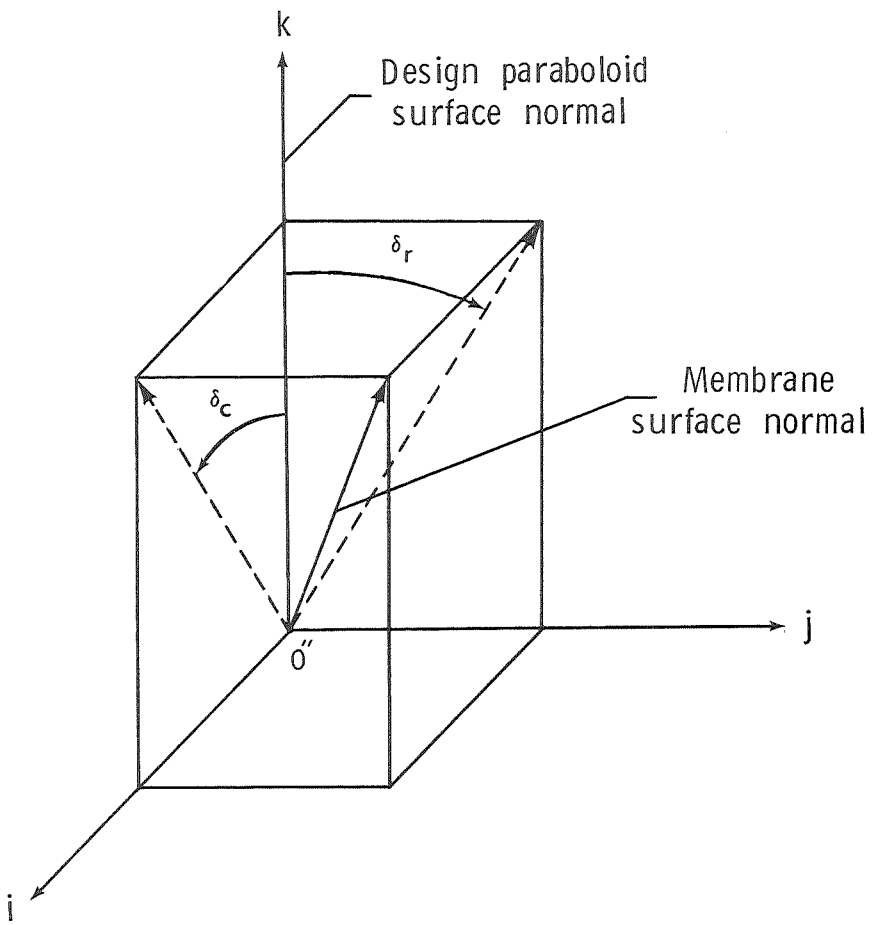

Figure 11.- Sketch defining membrane surface-slope errors.

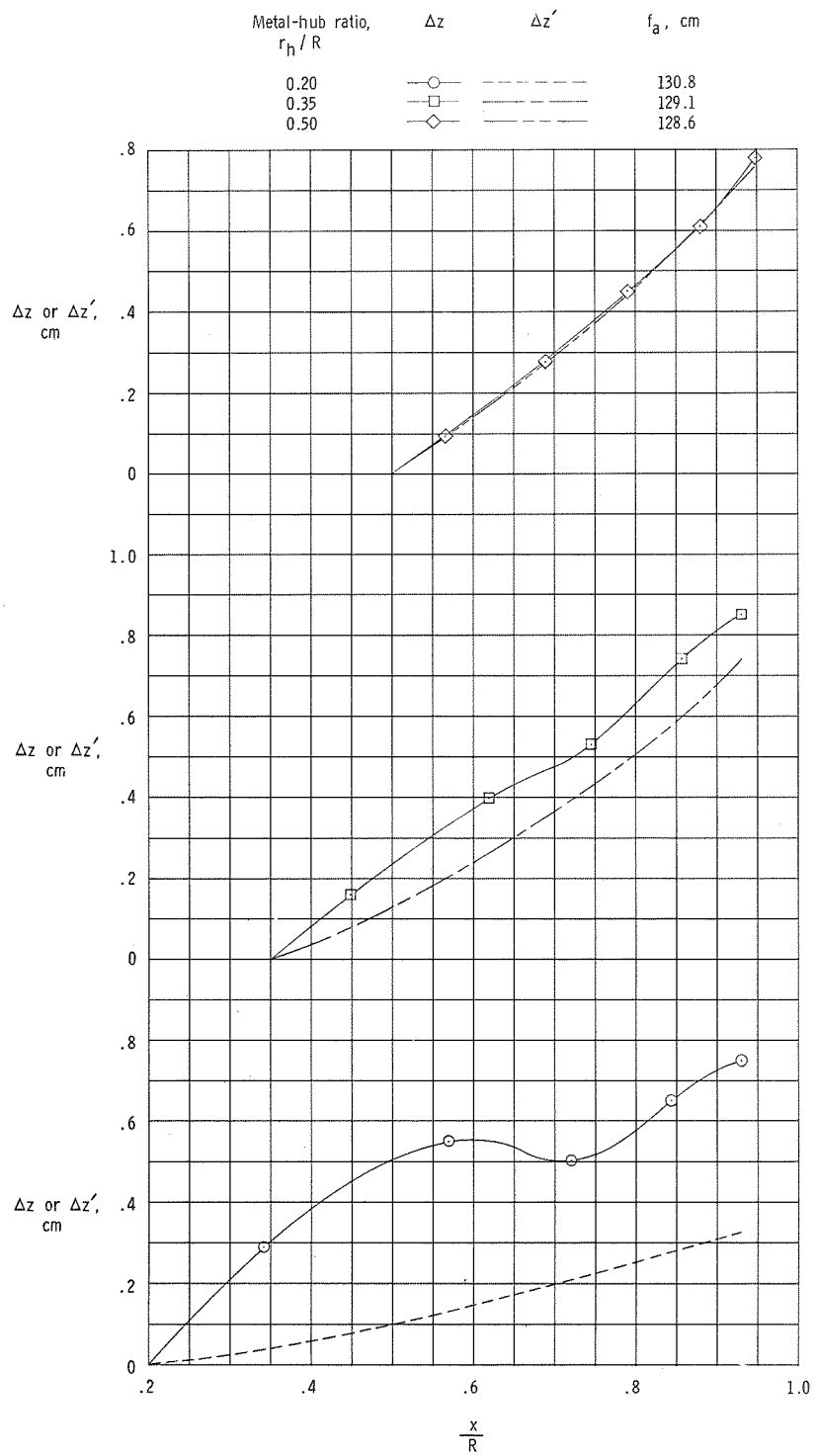

(a) Vertical displacement.

Figure 12.- Variation of membrane vertical displacements and radial-slope errors for three whirling-membrane models.

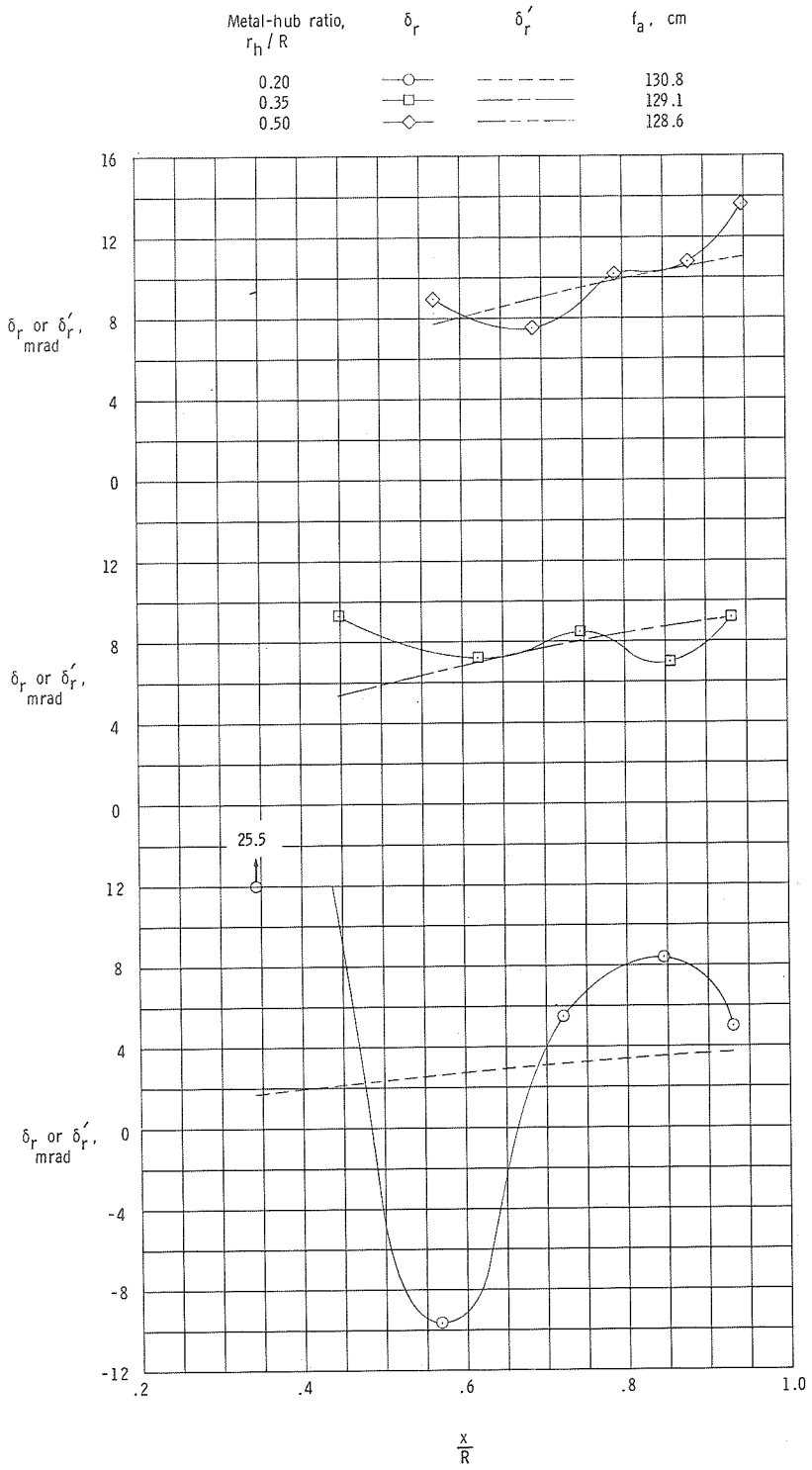

(b) Radial-slope error.

Figure 12.- Concluded.

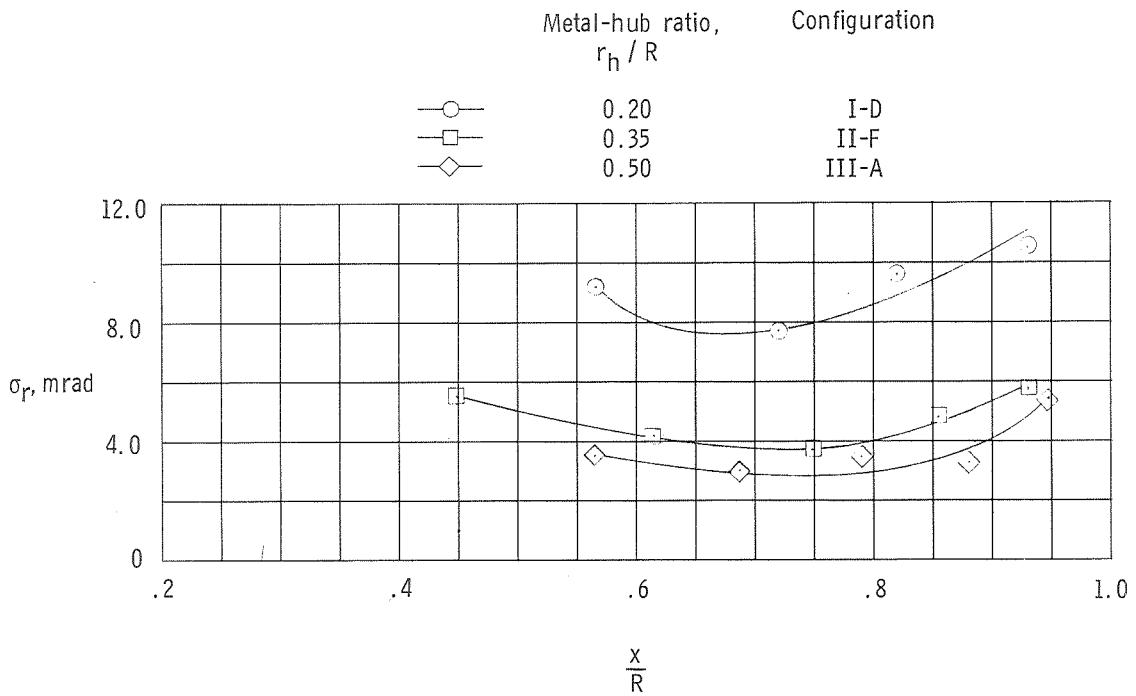

(a) Standard deviation of radial-slope error.

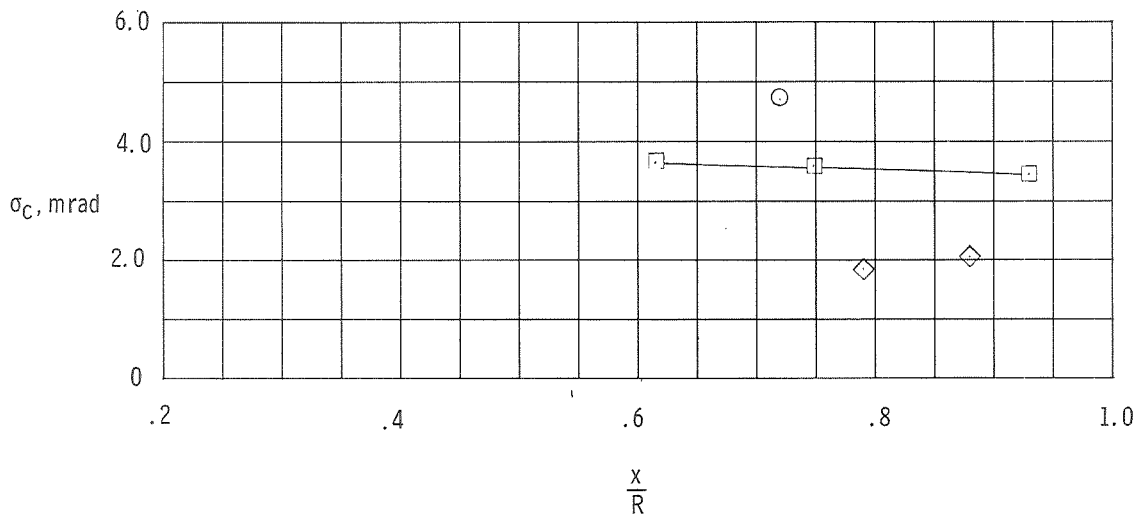

(b) Standard deviation of circumferential-slope error.

Figure 13.- Variation of standard deviation of radial- and circumferential-slope error for optimum configuration of the three hub models.

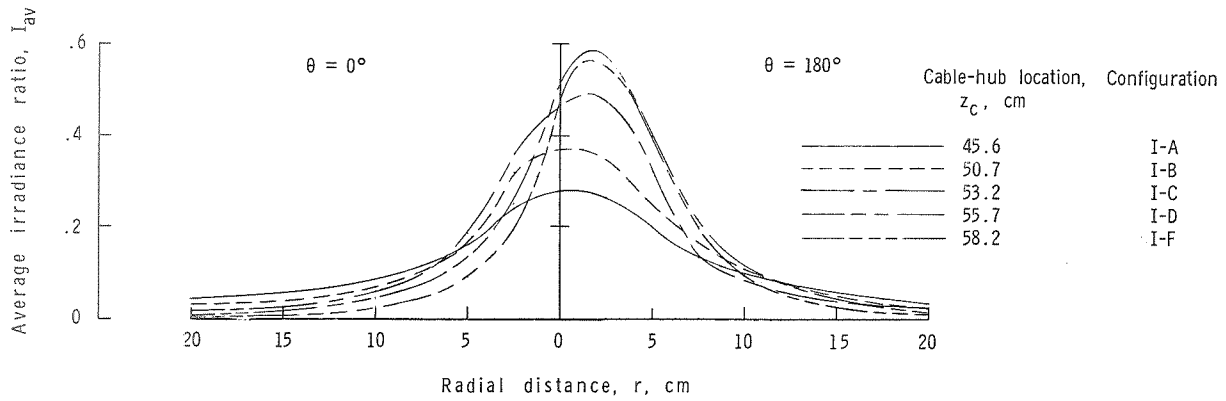

(a) 0.20R hub model.

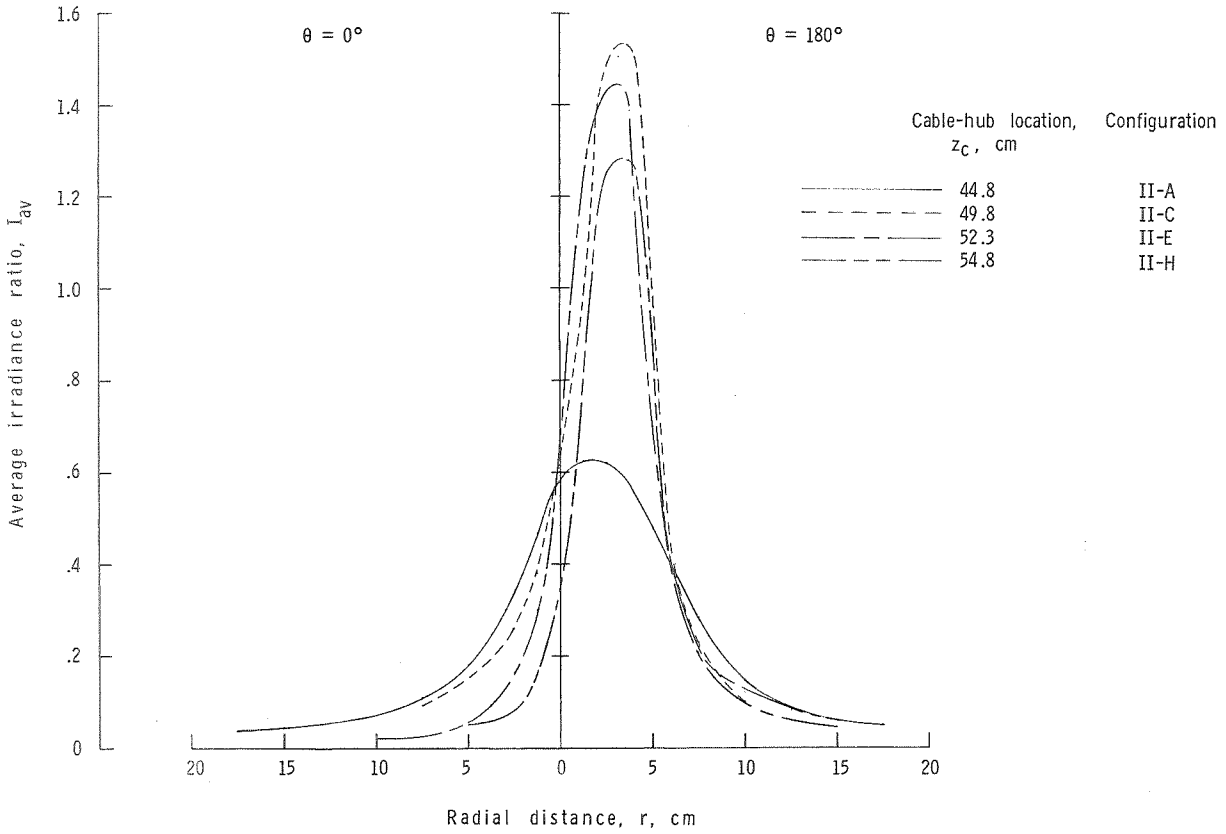

(b) 0.35R hub model.

Figure 14.- Average irradiance-ratio distributions along the $\theta = 0^{\circ}$-180° axis in or near the design focal plane.

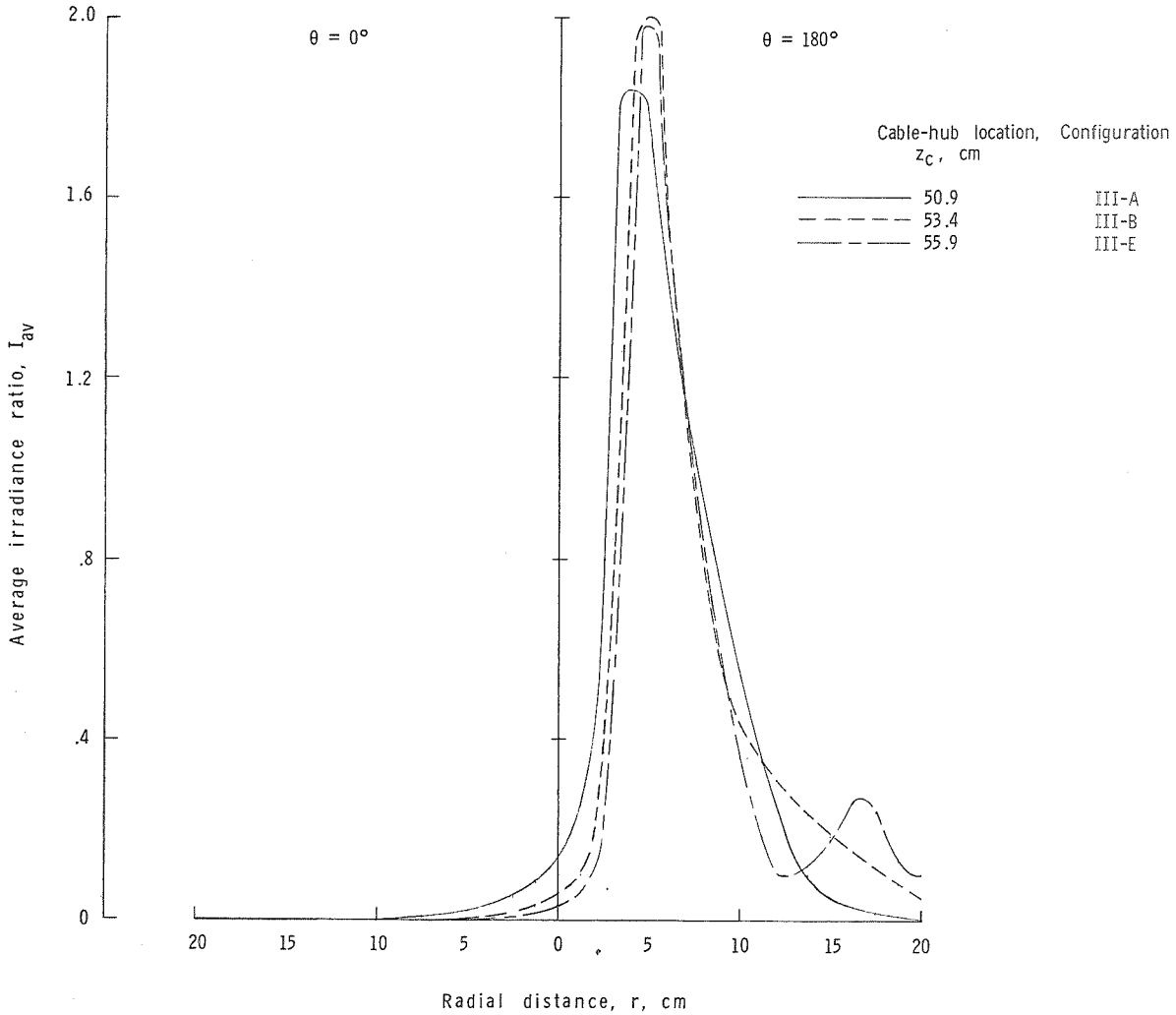

(c) 0.50R hub model.

Figure 14.- Concluded.

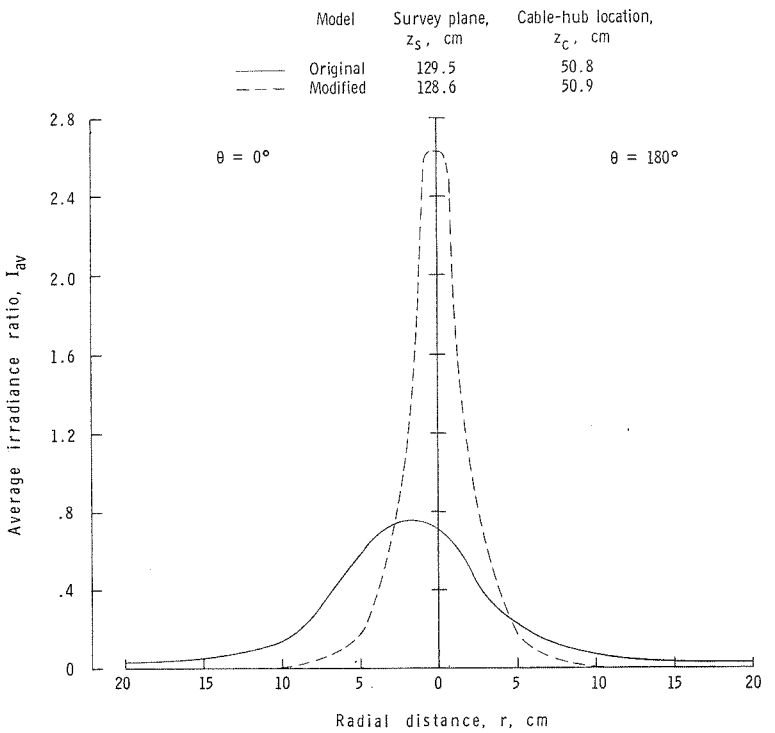

(a) θ = 0°-180° axis.

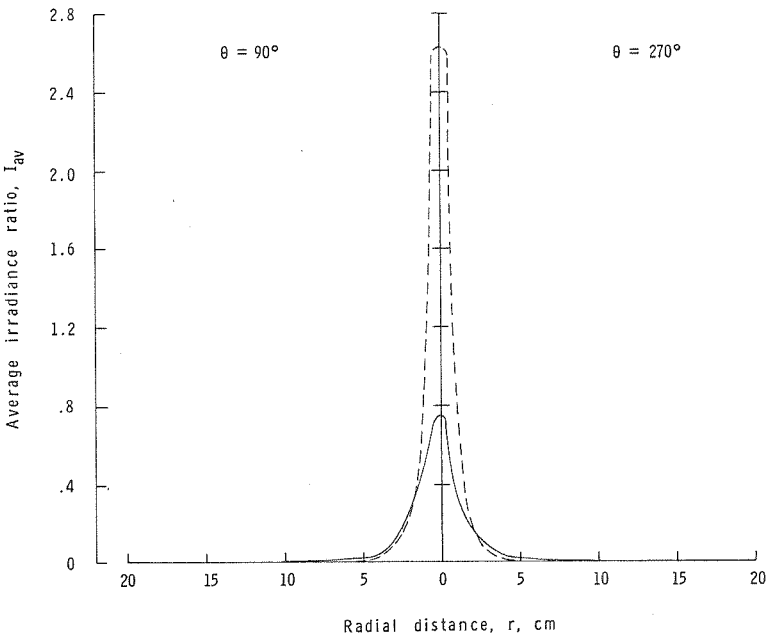

(b) θ = 90°-270° axis.

Figure 15.- Average irradiance-ratio distributions along θ = 0°-180° and θ = 90°-270° axes for the original and modified 0.50R hub models.

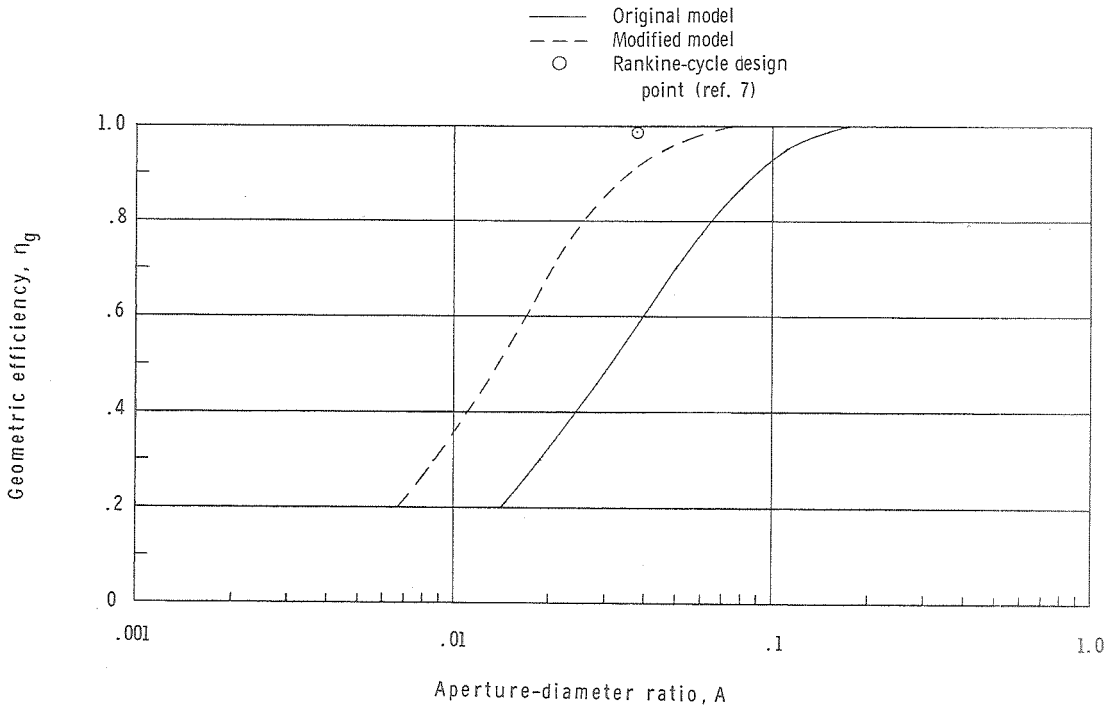

Figure 16.- Geometric efficiencies for the original and modified 0.50R hub models.

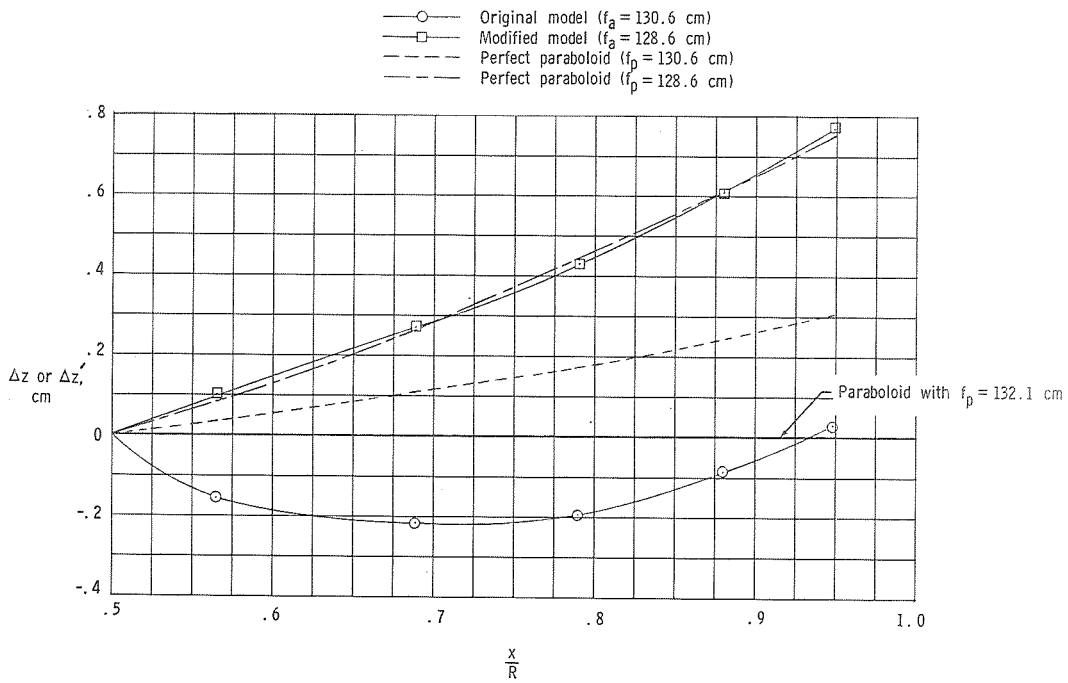

Figure 17.- Comparison of measured membrane deflections with membrane deflections for paraboloids having the same apparent focal lengths.

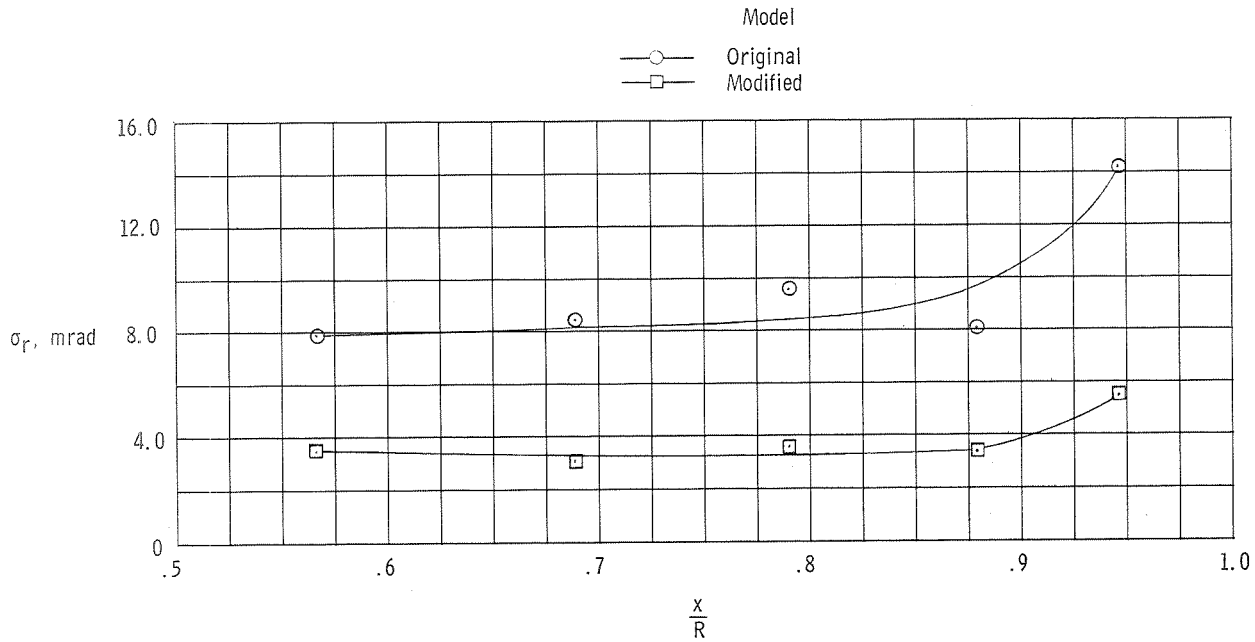

Figure 18.- Variation of standard deviation of radial-slope error for the original and modified 0.50R hub models.

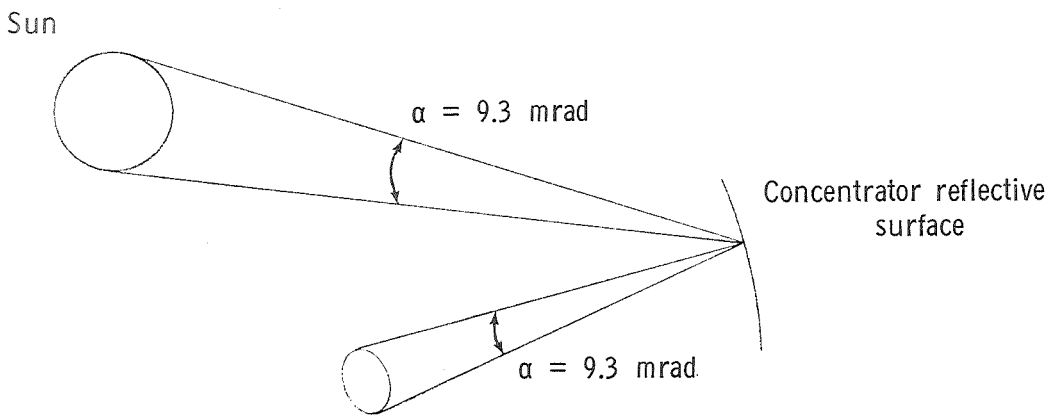

Figure 19.- Solar collimation angle.

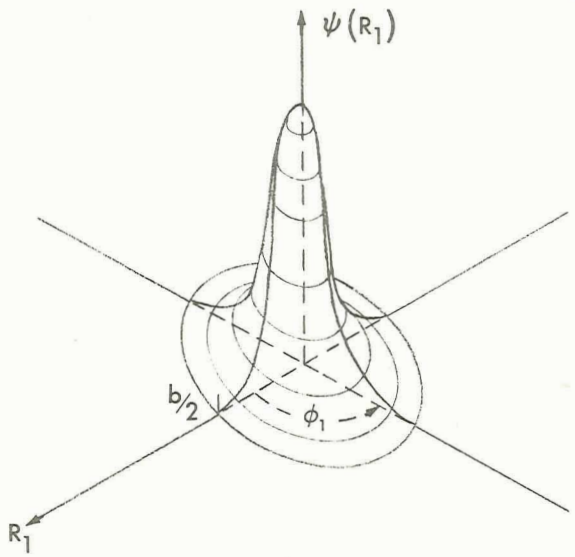

(a) Gaussian distribution.

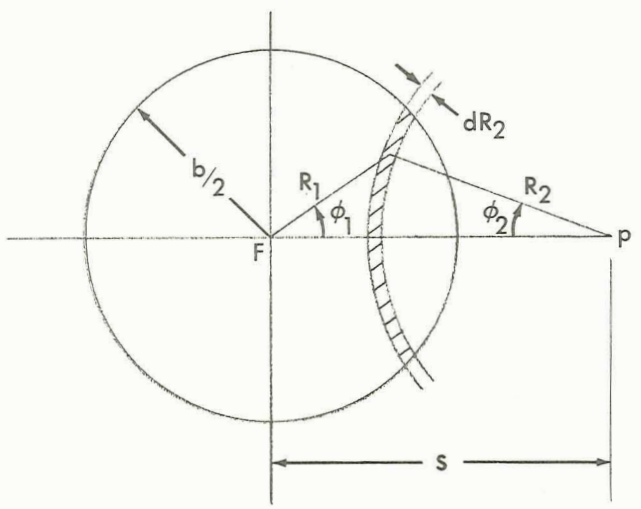

(b) Scattering circle and coordinate system.

Figure 20.- Gaussian distribution of reflected cone centers in focal plane of geometrically imperfect concentrator.

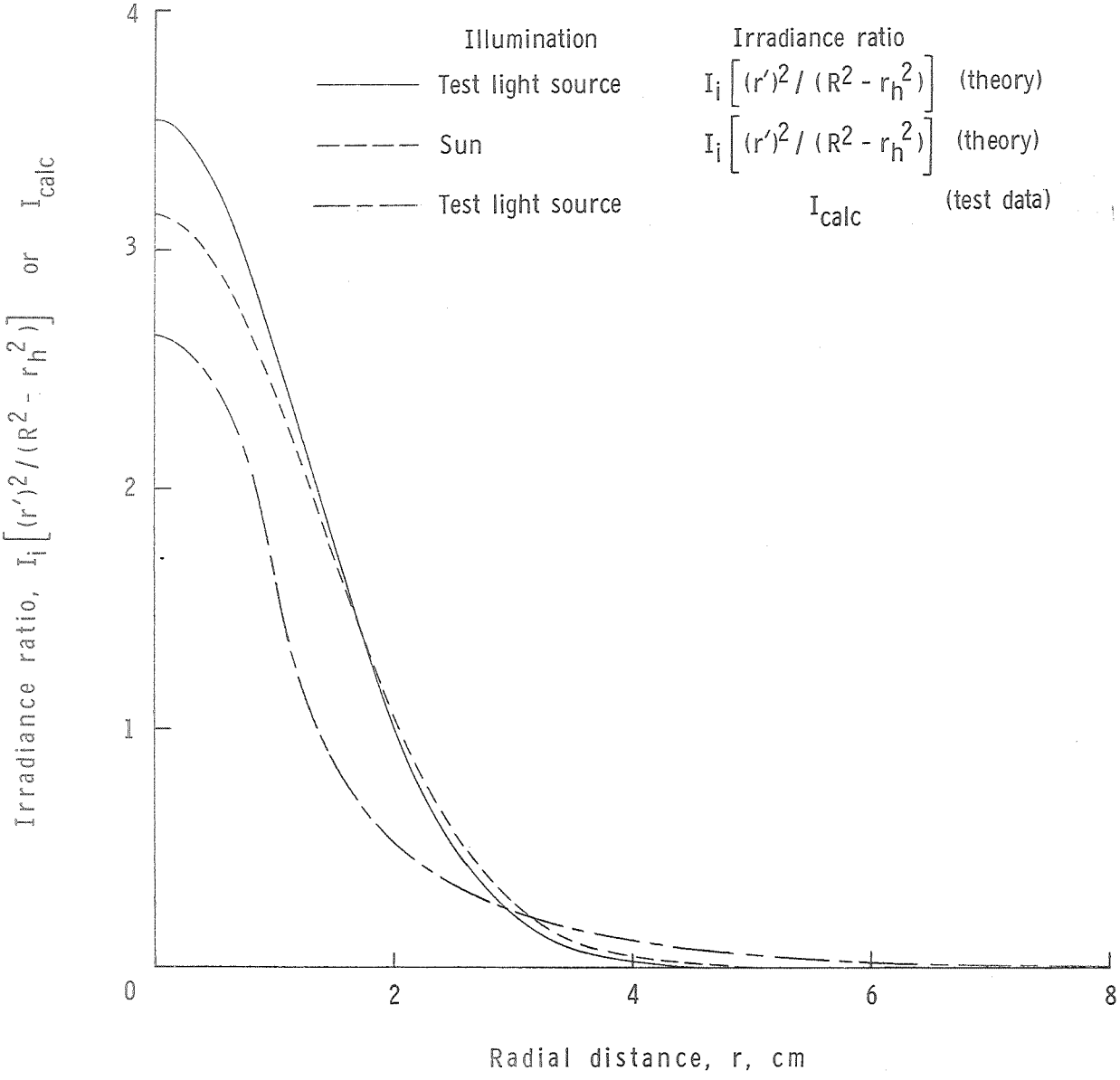

Figure 21.- Irradiance-ratio distributions for test-light and solar illumination.

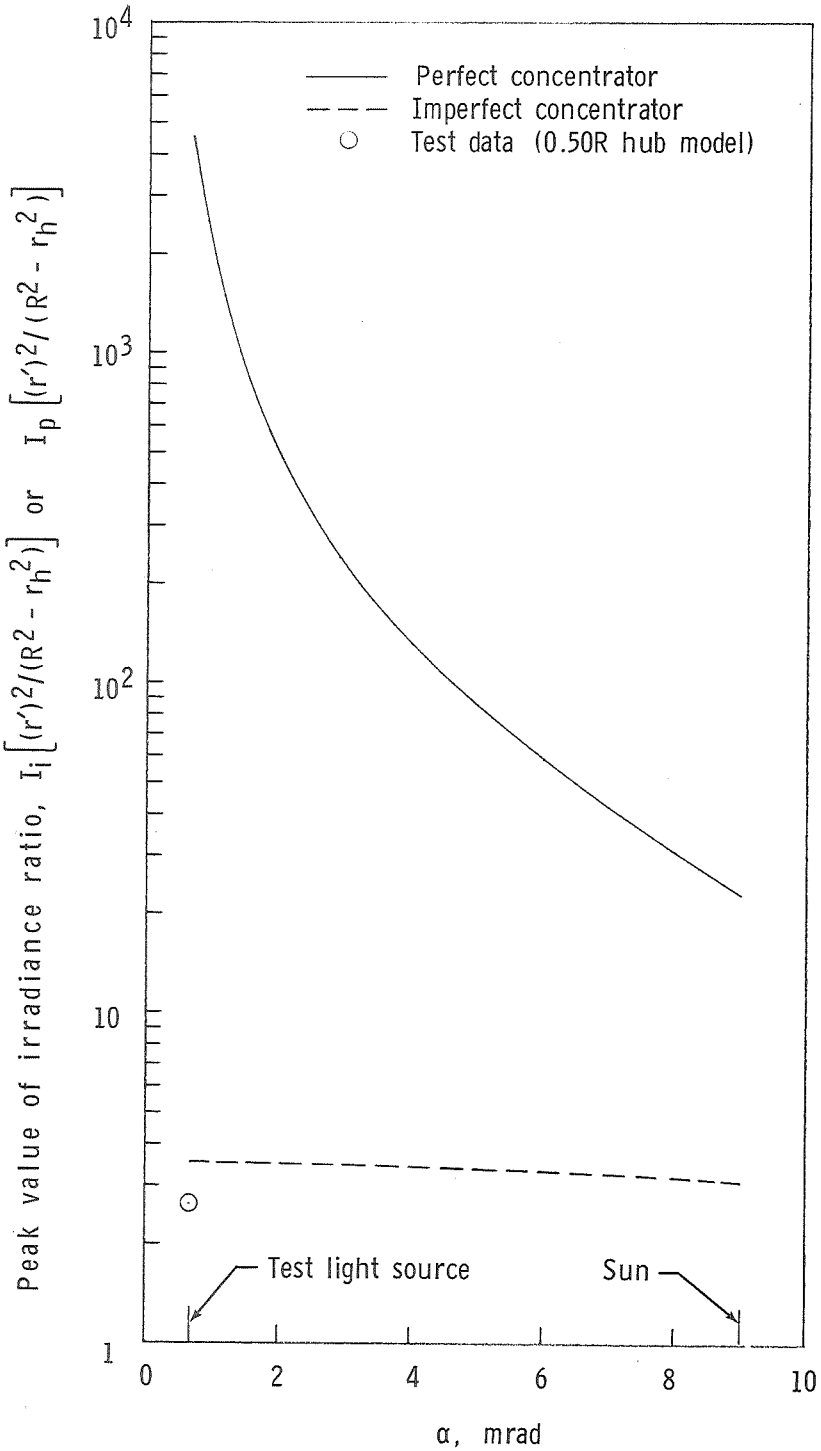

Figure 22.- Variation of peak irradiance ratio with collimation angle.

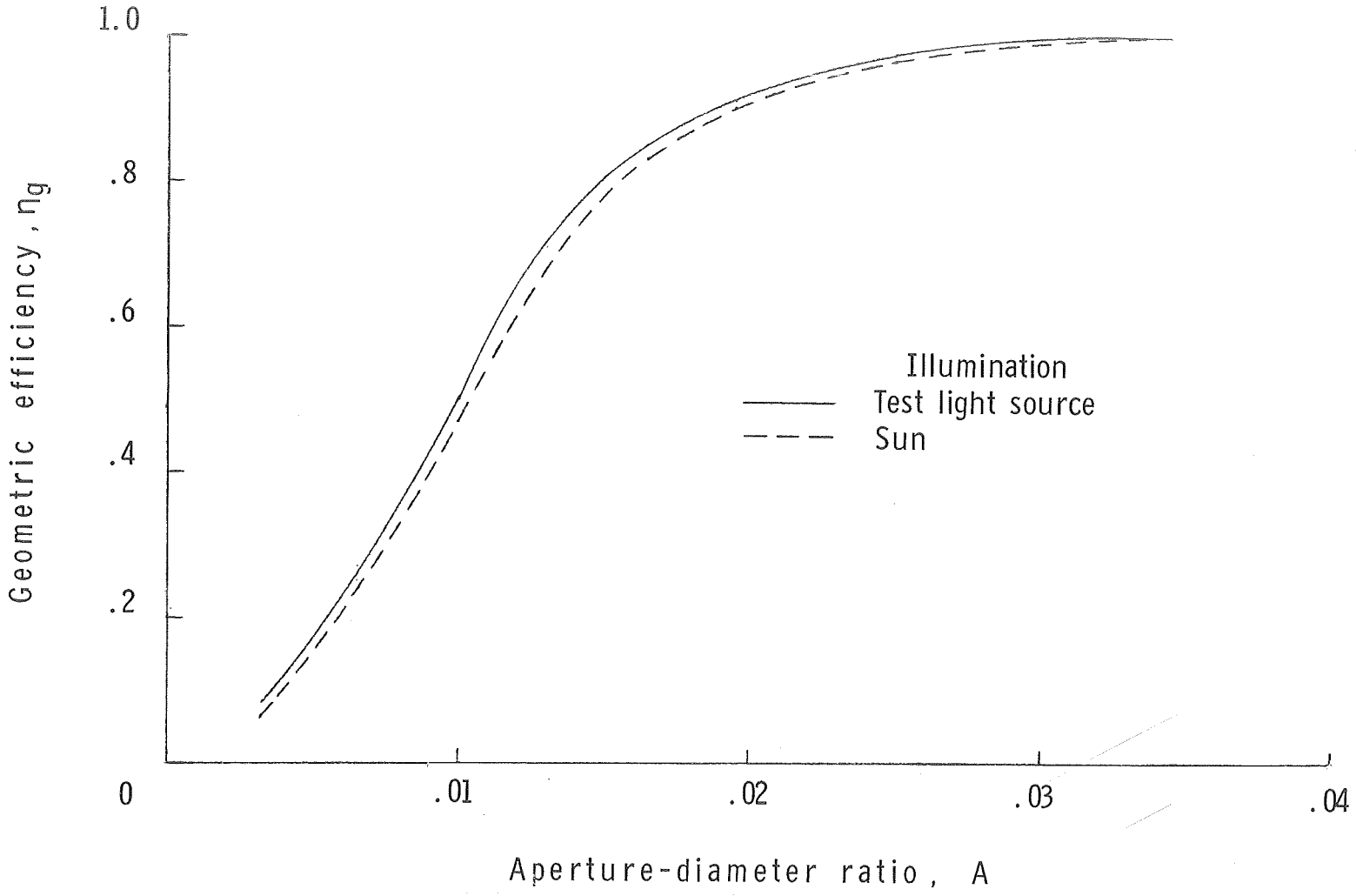

Figure 23.- Variation of geometric efficiency for test-light and solar illumination.

NATIONAL AERONAUTICS AND SPACE ADMINISTRATION
WASHINGTON, D. C. 20546

OFFICIAL BUSINESS

FIRST CLASS MAIL

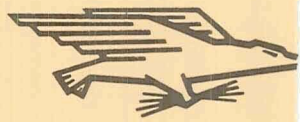

POSTAGE AND FEES PAID
NATIONAL AERONAUTICS AN
SPACE ADMINISTRATION

POSTMASTER: If Undeliverable (Section 158 Postal Manual) Do Not Return

"The aeronautical and space activities of the United States shall be conducted so as to contribute . . . to the expansion of human knowledge of phenomena in the atmosphere and space. The Administration shall provide for the widest practicable and appropriate dissemination of information concerning its activities and the results thereof."

—NATIONAL AERONAUTICS AND SPACE ACT OF 1958

NASA SCIENTIFIC AND TECHNICAL PUBLICATIONS

TECHNICAL REPORTS: Scientific and technical information considered important, complete, and a lasting contribution to existing knowledge.

TECHNICAL NOTES: Information less broad in scope but nevertheless of importance as a contribution to existing knowledge.

TECHNICAL MEMORANDUMS: Information receiving limited distribution because of preliminary data, security classification, or other reasons.

CONTRACTOR REPORTS: Scientific and technical information generated under a NASA contract or grant and considered an important contribution to existing knowledge.

TECHNICAL TRANSLATIONS: Information published in a foreign language considered to merit NASA distribution in English.

SPECIAL PUBLICATIONS: Information derived from or of value to NASA activities. Publications include conference proceedings, monographs, data compilations, handbooks, sourcebooks, and special bibliographies.

TECHNOLOGY UTILIZATION PUBLICATIONS: Information on technology used by NASA that may be of particular interest in commercial and other non-aerospace applications. Publications include Tech Briefs, Technology Utilization Reports and Notes, and Technology Surveys.

Details on the availability of these publications may be obtained from:

SCIENTIFIC AND TECHNICAL INFORMATION DIVISION

NATIONAL AERONAUTICS AND SPACE ADMINISTRATION

Washington, D.C. 20546